

Bath-induced Zeno localization in driven many-body quantum systems

Thibaud Maimbourg,^{1,*} Denis M. Basko,² Markus Holzmann,² and Alberto Rosso¹

¹*LPTMS, CNRS, Université Paris-Saclay, 91405, Orsay, France.*

²*Université Grenoble Alpes and CNRS, LPMMC, 25 rue des Martyrs, 38042 Grenoble, France*

We study a quantum interacting spin system subject to an external drive and coupled to a thermal bath of spatially localized vibrational modes, serving as a model of Dynamic Nuclear Polarization. We show that even when the many-body eigenstates of the system are ergodic, a sufficiently strong coupling to the bath may effectively localize the spins due to many-body quantum Zeno effect, as manifested by the hole-burning shape of the electron paramagnetic resonance spectrum. Our results provide an explanation of the breakdown of the thermal mixing regime experimentally observed above 4 – 5 Kelvin.

The fate of an isolated many-body quantum system, *i.e.* thermalization or ergodicity breaking, depends on the statistical properties of its eigenstates [1]. Indeed, the unitary dynamics projects, through dephasing, the initial state on the eigenstates of the Hamiltonian. According to the Eigenstate Thermalization Hypothesis (ETH), every eigenstate is representative of the ensemble; namely, the expectation value of physical observables in an eigenstate depends only upon a few conserved quantities (such as the total energy) and coincides with the prediction of the microcanonical ensemble [2–4]. It was recently realized that ETH may break down due to many-body localization (MBL, see recent reviews [5–7] and references therein), when Anderson localization in the many-body Hilbert space prevents the eigenstates from spreading ergodically over the available portion of the Hilbert space [8, 9].

In open systems, coupling to an external bath permits thermalization even when eigenstates are localized, as manifested by phonon-induced hopping transport of localized electrons [10]: the bath supplies or absorbs the energy needed to allow hopping between localized states, thereby destroying the localization. In this Letter, we show how coupling to a local bath can instead induce localization in a quantum many-body system with ergodic eigenstates, as revealed by the properties of the nonequilibrium steady state reached under an external drive. Such localization is not due to Anderson, but rather to the quantum Zeno effect [11–17] in the many-body Hilbert space. This scenario should not be confused with the quantum Zeno effect in quantum gases with localized particle losses [18–21] or dephasing [22], where the combined effect of local single-particle losses and many-body interactions is mainly to renormalize single-particle quantities. It should also not be mistaken with localization induced by subohmic baths at zero temperature [23–26], essentially a polaronic effect destroyed by interactions or finite temperature [27]. The localization studied here is more akin to the entanglement transition between volume-law and area-law phases found in schematic models with random local projective measurements such as quantum circuits [28–36], free fermionic chains [37] and interacting bosonic chains [38–40].

We use an out-of-equilibrium driven-dissipative protocol: it has recently been emphasized [41–46] and experimentally confirmed [47] that fingerprints of thermalization or localization appear in the steady state of systems weakly coupled to a bath if an external drive is

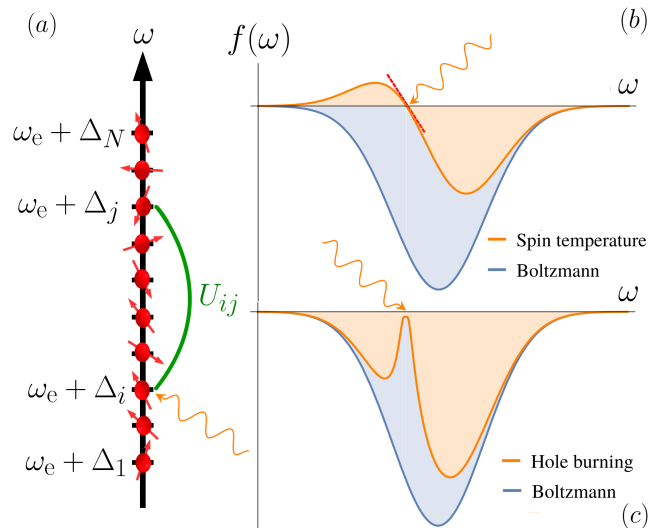


FIG. 1. (a) Sketch of the system: N electron spins with dipolar interactions of strength U_{ij} in a strong inhomogeneous magnetic field $\omega_e + \Delta_i$ in contact with a thermostat are irradiated by microwaves at frequency ω_{MW} (wavy arrow). (b)(c) EPR spectrum $f(\omega)$ at Boltzmann equilibrium (blue curve) and under microwave driving displaying two different shapes (orange curves): (b) the spin-temperature profile [48, 49] with a linear behavior (dashed red) of slope $\beta_s/2$ close to microwave resonance ($\omega = \omega_{\text{MW}}$) (c) the hole burning at microwave resonance.

applied. In fact, if the transitions rates induced by the bath or drive are small with respect to dephasing, the dynamics still gets projected in the Hamiltonian eigenstates. For thermal systems, the steady state is then a mixture of ETH-satisfying eigenstates. Thus, even in the presence of a drive, it is described by an effective equilibrium with a unique temperature. On the contrary, driven MBL systems end up in a non-thermal steady state.

Through a driven protocol we show that a bath of spatially-localized modes triggers spatially-localized quantum jumps of the system's state during its evolution which can induce localization in ETH systems. Indeed if the bath transition rates prevail over dephasing, the projection on eigenstates is hindered, preventing the system from reaching a thermal stationary state. Consequently an effective equilibrium description of the steady state breaks down. Note that the bath transition rates are generally increasing with temperature; thus, curiously, localization happens in a high-temperature phase. The phenomenon is analog to the quantum Zeno effect, when the unitary evolution is impeded by infinitely frequent measurements of a coupled probe. Here the spatially-localized quantum jumps play the

* thibaud.maimbourg@lptms.u-psud.fr

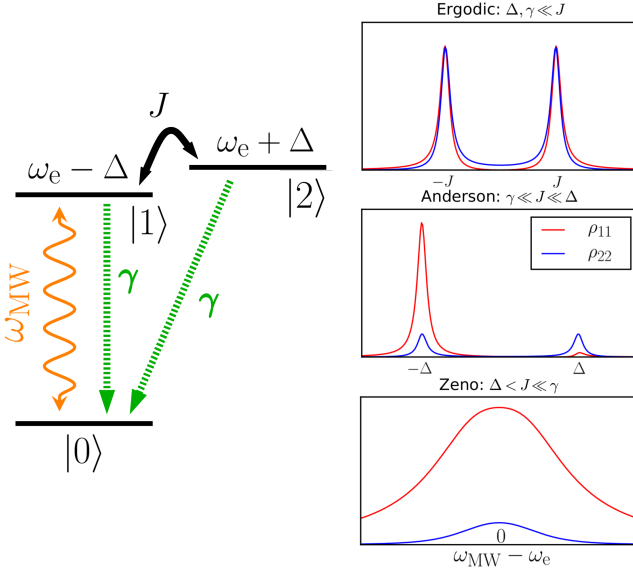


FIG. 2. (left) A system of three levels $|0\rangle, |1\rangle, |2\rangle$ with energies $0, \omega_e \pm \Delta$ and a coupling J between $|1\rangle$ and $|2\rangle$. A monochromatic drive at frequency ω_{MW} couples $|0\rangle$ and $|1\rangle$. Two independent zero-temperature baths lead to decay of the population from $|1\rangle$ and $|2\rangle$ to $|0\rangle$ with rate 2γ . The largest energy scale is ω_e . (right) Level populations $\rho_{ii}(\omega_{\text{MW}} - \omega_e)$ in three limits. In the Anderson limit the strong imbalance between ρ_{11} and ρ_{22} is caused by the eigenstates' localization on the respective levels. In the Zeno limit the system eigenstates are uniformly spread over $|1\rangle$ and $|2\rangle$, but they do not have time to form because of the dissipation.

role of the measurements. The essence of the difference between the Zeno and the Anderson localization in a driven-dissipative system can be illustrated by a simple example with just three levels, shown in Fig. 2.

We investigate these ideas in the problem of Dynamic Nuclear Polarization (DNP) [49] induced by the nonequilibrium steady state of N diluted electron spins exposed to a strong magnetic field ω_e ¹ along the z axis. Their Hamiltonian reads (see Fig. 1(a))

$$\hat{H}_S = \sum_{i=1}^N (\omega_e + \Delta_i) \hat{S}_i^z + \hat{H}_{\text{dip}} \quad (1)$$

Here Δ_i is a small disorder from the random orientation of the molecule where the spin lies and \hat{H}_{dip} stands for the dipolar interaction. The large value of the magnetic field implies $\hat{S}^z = \sum_i \hat{S}_i^z$ is conserved, hence the dipolar Hamiltonian gets truncated as [42, 49–51]

$$\hat{H}_{\text{dip}} = \sum_{i < j} U_{ij} \left(\hat{S}_i^+ \hat{S}_j^- + \hat{S}_i^- \hat{S}_j^+ - 4 \hat{S}_i^z \hat{S}_j^z \right) \quad (2)$$

where U_{ij} depends on the distance between the spins and their orientation with respect to the magnetic field. The sample is at temperature β^{-1} and driven by monochromatic microwave irradiation at frequency ω_{MW} . This protocol is important for NMR applications as when $\omega_{\text{MW}} \approx \omega_e$, the electron spins reach a stationary state that hyperpolarize the nuclear spins of the sample. The steady-state properties are probed experimentally by measuring the Electron Paramagnetic

Resonance (EPR) spectrum which displays two typical shapes:

- a linear curve close to irradiation frequency (Fig. 1(b)). This shape tells that the electrons are effectively at equilibrium at temperature β_s^{-1} (called *spin temperature*) interacting via \hat{H}_S with a shifted magnetic field $\omega_e \rightarrow \omega_e - h$ where $h \simeq \omega_{\text{MW}}$. In this so-called *thermal mixing* regime, all nuclear species (1H , ^{13}C , ^{15}N ...) thermalize at β_s and hyperpolarization occurs if $\beta_s \gg \beta$.

- a “hole burning” close to irradiation (Fig. 1(c)). This shape was found by Bloch [52] for non-interacting spins: the spins at resonance with the microwaves ($\omega_e + \Delta_i \simeq \omega_{\text{MW}}$) are brought to a high temperature while the off-resonant ones remain at β^{-1} . The hole-burning shape is recovered in the MBL regime [41–45], revealing different local temperatures. In this situation the nuclear species exhibit weak polarization not accounted by a single temperature.

Thermal mixing usually occurs around $\beta^{-1} = 1$ K and the spin-temperature shape was observed long ago in the EPR spectrum of Ce^{3+} in a CaWO_4 crystal [48]. More recently, experiments on irradiated EPR spectrum retrieved instead a hole-burning shape [53–55] above 4–5 K. At this higher temperature, the system-bath interaction becomes more effective as bath timescales shorten. In this Letter we argue that this high-temperature hole-burning shape originates from the interaction with the bath and not from the MBL. In particular, we compute the EPR spectrum and show a crossover from a spin-temperature to a hole-burning shape simply by increasing β^{-1} . We interpret this crossover as a manifestation of a bath-induced Zeno localization in the many-body eigenbasis of $\{\hat{S}_i^z\}$.

Effective dynamics due to the bath – The electron spins are dilute, so we assume they are in contact with independent spatially-localized vibration modes \hat{B}_i^μ ²:

$$\hat{H}_{\text{int}} = \sum_{\substack{i=1, \dots, N \\ \mu=x, y, z}} \hat{S}_i^\mu \otimes \hat{B}_i^\mu \quad (3)$$

The quantum dynamics of the spin and bath degrees of freedom amounts to an intractable unitary evolution of the full density matrix $\rho_{S \otimes B}$. Nonetheless, assuming the bath is equilibrated at temperature β^{-1} , one may trace out the \hat{B}_i^μ variables and write an effective evolution for the spin system density matrix $\rho = \text{Tr}_B(\rho_{S \otimes B})$. The ensuing evolution is no longer unitary but must still preserve the trace and semi-positivity of ρ . The most general Markovian dynamics must then be of the Gorini-Kossakowski-Sudarshan-Lindblad (GKSL) form [16]:

$$\dot{\rho} = -i[\hat{H}, \rho] + \sum_{\alpha} \hat{A}_{\alpha} \rho \hat{A}_{\alpha}^\dagger - \frac{1}{2} \left\{ \hat{A}_{\alpha}^\dagger \hat{A}_{\alpha}, \rho \right\} \quad (4)$$

where \hat{H} is Hermitian and $\{\hat{A}_{\alpha}\}$ is a set of jump operators. To integrate the bath degrees of freedom [SM, Sec. I], we consider the spin-bath coupling weak and perform a perturbative expansion of the full unitary dynamics of $\rho_{S \otimes B}$ at second order in \hat{H}_{int} . Within the Born-Markov approximation [16, 56, 57], one can turn the perturbative expansion into an effective Markovian evolution for ρ . As the bath degrees

¹ Units are such that $k_B = 1$, $\hbar = 1$.

² See the Supplementary Material [SM] for further details.

of freedom are independent, they enter the dynamical equation only through a single equilibrium correlation function

$$\gamma(\omega) = \int_{-\infty}^{\infty} d\tau e^{i\omega\tau} \left\langle \hat{B}_i^\mu(\tau) \hat{B}_i^\mu(0) \right\rangle_B = \frac{h(\omega)}{T(|\omega|)}. \quad (5)$$

The hypothesis of an equilibrated bath implies the last equality, in which $h(\omega) = (1 + e^{-\beta\omega})^{-1}$ enforces detailed balance at inverse temperature β , while $T(|\omega|)$ is the timescale of the exchange of energy ω with the spins.

The way to implement the Markovian approximation is not unique, yielding different dynamical equations in general not of the GKSL form (4). A Markovian prescription was recently proposed [58–60], which leads to a GKSL form by setting the unitary part $\hat{H} = \hat{H}_S$ ³ and the jump operators of the dissipative part

$$\hat{A}_\alpha = \sum_{n,m} \sqrt{\gamma(\omega_{nm})} \langle m | \hat{S}_i^\mu | n \rangle | m \rangle \langle n | \quad (6)$$

with $\alpha = (i, \mu)$ and $\omega_{nm} = \varepsilon_n - \varepsilon_m$ are energy gaps of \hat{H}_S . We have three characteristic timescales $T(|\omega|)$ corresponding to three energy scales: (i) T_1 for transitions of energy gap $\pm\omega_e$, providing the jump operators

$$\begin{aligned} \hat{A}_i^x &= \sqrt{\frac{h(\omega_e)}{2T_1}} \left(\hat{S}_i^- + e^{-\beta\omega_e/2} \hat{S}_i^+ \right) \\ \hat{A}_i^y &= i\sqrt{\frac{h(\omega_e)}{2T_1}} \left(\hat{S}_i^- - e^{-\beta\omega_e/2} \hat{S}_i^+ \right), \end{aligned} \quad (7)$$

(ii) T^* for transitions of finite energy $|\omega| \ll \omega_e$, and (iii) $T(0)$ for zero-energy transitions within the same eigenstate, giving

$$\hat{A}_i^z = \frac{\hat{S}_i^z}{\sqrt{2T^*}} + \left(\frac{1}{\sqrt{2T(0)}} - \frac{1}{\sqrt{2T^*}} \right) \sum_n \langle n | \hat{S}_i^z | n \rangle | n \rangle \langle n |. \quad (8)$$

The operators (7) and (8) (when $T(0) \approx T^*$) are well localized in space and called nonsecular jump operators. The quantum trajectories thus result from a competition between the unitary dynamics which, through dephasing, projects the system's state on thermal eigenstates, and repeated measurements performed by the nonsecular jump operators. If the jump rates dominate the dephasing, the system's projection on thermal eigenstates is hence hampered in a way reminiscent of the quantum Zeno effect.

This choice of jump operators contrasts with the Markovian prescription employed in the usual weak-coupling scheme [16, 56, 57]. Within this approach, the GKSL form of master equation (4) is actually recovered through an additional secular approximation where the jump operators select only a given transition of energy ω_{nm} between eigenstates $|m\rangle$ and $|n\rangle$:

$$\hat{A}_\alpha^{\text{sec}}(\omega_{nm}) = \sqrt{\gamma(\omega_{nm})} \langle m | \hat{S}_i^\mu | n \rangle | m \rangle \langle n | \quad (9)$$

Note that the secular jump operators (9) are projected on the eigenbasis of \hat{H}_S ; if the eigenstates satisfy ETH, the jump operators are delocalized in space. Inserting

them in Eq. (4) yields an exponential decay of the off-diagonal elements (coherences) in the eigenbasis:

$$\dot{\rho}_{nm} = - \left(i\omega_{nm} + \frac{1}{T_{nm}} \right) \rho_{nm} \quad (10)$$

where $i\omega_{nm}$ is the dephasing due to the unitary evolution and $T_{nm} > 0$ is the decoherence [SM, Sec.I.B] induced by the bath timescales. Therefore one can work in the *Hilbert approximation* where the dynamics is projected on the diagonal elements only: it amounts to transit from an eigenstate to the other with rates given in [SM, Sec.I.E]. The nonsecular dynamics (6) adds to the right-hand side of Eq. (S48) other entries than ρ_{nm} , with associated bath rates [SM, Sec.I.F], allowing the existence of coherences in the steady-state solution. The Hilbert approximation is thus retrieved within the nonsecular dynamics when the bath timescales are long with respect to dephasing.

Microwave drive – In equilibrium, the steady state is described by the Boltzmann distribution with either choice of jump operators. The nonsecular evolution brings drastic changes out of equilibrium: in a DNP protocol the system is irradiated by microwaves described by $\hat{H}_{\text{MW}}(t) = \omega_1 \left[\hat{S}^x \cos(\omega_{\text{MW}}t) + \hat{S}^y \sin(\omega_{\text{MW}}t) \right]$. The time dependence is handled using a rotating frame at frequency ω_{MW} where the microwaves are stationary. The dynamics of the rotated density matrix $e^{i\omega_{\text{MW}}t\hat{S}^z} \rho(t) e^{-i\omega_{\text{MW}}t\hat{S}^z} \rightarrow \rho(t)$ remains given by Eq. (4) with the shift $\hat{H} = \hat{H}_S - \omega_{\text{MW}}\hat{S}^z + \omega_1\hat{S}^x$ [SM, Sec.I.D].

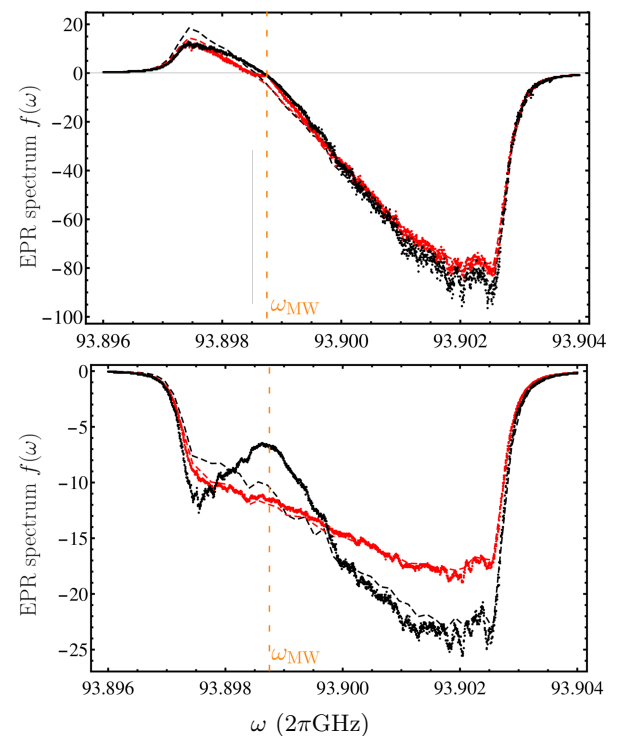


FIG. 3. EPR spectra : dots represent numerical profiles for Hilbert (red) and nonsecular (black) evolutions. Dashed lines are calculated through a spin-temperature ansatz. (top) $\beta^{-1} = 1.2$ K. The bath is slow and as a consequence nonsecular and Hilbert dynamics yield similar spin-temperature curves. (bottom) $\beta^{-1} = 12$ K. The bath timescales are short and the full (nonsecular) dynamics gets localized and displays the hole burning. Here the Hilbert approximation fails, predicting a spin-temperature behavior. Averages are done over 1000 realizations.

³ A Hermitian Lamb-shift operator should be added to \hat{H}_S . We show in [SM] that it is negligible for our system.

Numerical computation of the EPR spectrum – We are interested in comparing the stationary states predicted by the Hilbert dynamics with the ones obtained by the nonsecular evolution Eq. (4) with jumps (7),(8). In our numerics, the disorder Δ_i is drawn uniformly in the interval $[-\frac{\Delta\omega_e}{2}, \frac{\Delta\omega_e}{2}]$ and the dipolar couplings ⁴ U_{ij} are mimicked by independent Gaussian distributions with zero mean and variance U^2/N , with U of the same order of magnitude as $\Delta\omega_e$. We fix the disorder $\Delta\omega_e = 5 \cdot 2\pi\text{MHz}$ and $U = 0.75 \cdot 2\pi\text{MHz}$ (note that $\omega_e = 93.9 \cdot 2\pi\text{GHz}$) where \hat{H}_S has ETH statistics. We consider two temperatures ; at high temperature the characteristic times of the bath are short (see Table I).

$\beta^{-1}(\text{K})$	$T(0)(\mu\text{s})$	$T^*(\mu\text{s})$	$T_1(\mu\text{s})$	$\omega_1(2\pi\text{MHz})$	$\omega_{\text{MW}}(2\pi\text{GHz})$
1.2	1.6	80	160	0.628	93.8988
12	0.16	0.16	1.6	0.628	93.8988

TABLE I. Bath and microwaves control parameters chosen for the system at two temperatures, close to experimental orders of magnitude [41, 55, 61].

We compute numerically the steady-state density matrix ρ_{stat} [62]. The Hilbert case amounts to a $2^N \times 2^N$ linear system, which for $N = 10$ spins is sufficiently small to be treated by exact diagonalization. The nonsecular dynamics Eq. (4) is instead a $4^N \times 4^N$ linear system which requires the use of Krylov subspace methods (namely the biconjugate gradient stabilized algorithm) [63]. To probe the stationary state we focus on the EPR spectrum. The EPR experiment starts at time $\tau = 0$ by a $\pi/2$ microwave pulse that projects the steady-state polarization of a given spin i on the y axis: $\rho_{\pi/2} = e^{i\frac{\pi}{2}\hat{S}_i^x} \rho_{\text{stat}} e^{-i\frac{\pi}{2}\hat{S}_i^x}$. For short times after the pulse, the evolution is unitary and the polarization in the (x, y) plane is encoded in

$$g_i(\tau) = -2i\text{Tr} \left[\hat{S}_i^+(\tau) \rho_{\pi/2} \right] \quad (11)$$

where $\hat{S}_i^+(\tau) = e^{i\hat{H}_S\tau} \hat{S}_i^+ e^{-i\hat{H}_S\tau}$. The EPR spectrum is then defined by the Fourier transform $f(\omega) = \frac{1}{N} \sum_i \text{Re} \left[\int_0^\infty \frac{d\tau}{\pi} g_i(\tau) e^{-i\omega\tau} \right]$, explicitly calculated in [SM,Sec.II].

The EPR spectra are shown in Fig. 3. At low temperature, we observe a spin-temperature curve for both dynamics. Here the bath timescales are long with respect to dephasing. Consequently, the density matrix still gets projected in the eigenstate basis, yielding a similar situation as in the Hilbert approximation. At higher temperature, the EPR spectrum is spin-temperature-like for Hilbert dynamics, whereas it has a hole-burning shape in the nonsecular evolution. The spin-temperature behavior observed in the Hilbert approximation is expected [41–43] : due to the ETH, the jump operators projected on the eigenstates induce changes in energy and polarization without any other information such as the spatial location of the spins. On the contrary, in the nonsecular equation the jump operators are well localized in space and compete with

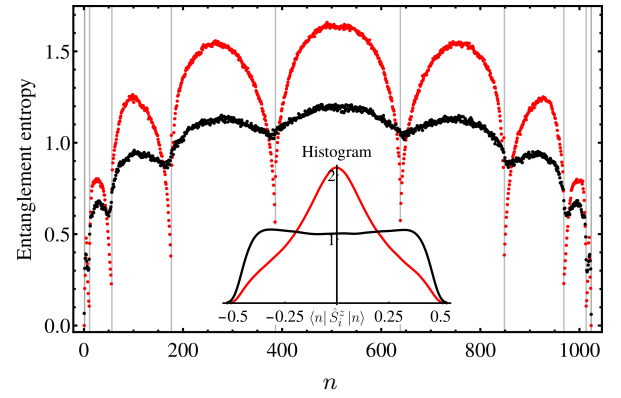


FIG. 4. (main) Entanglement entropy of the eigenstates of ρ_{stat} (red : Hilbert, black : nonsecular) classified by increasing energy. To compute it, we performed a partial trace of each eigenstate $|n\rangle\langle n|$ over spins 5 to 10. Vertical gray lines delimit sectors of constant polarization s_n^z . (inset) Smoothed histogram of S_i^z expectation values ($i = 1, \dots, N$) for 100 eigenstates in the middle of the $s_n^z = 0$ sector. For the Hamiltonian eigenstates, the local observable is peaked around its thermal value ($S_i^z \simeq 0$) as required by ETH. The nonsecular eigenstates present instead strong fluctuations, as for MBL states. Parameters correspond to those of Fig. 3(bottom).

the dephasing, which is not able to project the system on the eigenstates. The EPR spectrum becomes similar to the MBL case, although the eigenstates of \hat{H}_S are ergodic for the chosen parameters. The spin-temperature picture no longer holds and one can regard this breakdown as a type of Zeno localization induced by the bath. This breakdown is confirmed by comparing the EPR profiles with the ones (dashed lines in Fig. 3) obtained through a spin-temperature ansatz for the steady state density matrix $\rho_{nn}^{\text{ans}}(\beta_s, h) \propto e^{-\beta_s(\epsilon_n - hs_n^z)}$ where the spin temperature β_s is conjugated to the energy and the magnetic field h is conjugated to the polarization (s_n^z are the eigenvalues of the conserved \hat{S}^z). These parameters are computed by a fitting method introduced in [42] and recalled in [SM,Sec.III.B].

Spectral properties – The localization phenomenon exhibited by the experimentally relevant EPR spectra can be revealed through other observables. For instance, in [SM,Sec.III] we display the polarization profiles. In Fig. 4, we focus instead on the spectral properties of ρ_{stat} . We compare the entanglement entropy of the ρ_{stat} eigenstates in the Hilbert and nonsecular cases. The latter case is much less entangled and similar to MBL eigenstates [SM,Sec.III.D]. The present scenario is analog to the entanglement transition between volume-law and area-law phases analyzed in Refs. [28–40]. However we stress that the bath-induced localization unveiled here is very different from the localization studied in Refs. [41–46] and experimentally observed in [47]. In that case it is caused by MBL eigenstates that stem from a strong disorder (or weak interaction). In [SM,Sec.III.C] we show that in presence of MBL eigenstates, the nonsecular terms are negligible irrespective of temperature : Hilbert dynamics is therefore sufficiently accurate.

Conclusion – We have shown that bath transitions induced by localized vibrations compete with the dephasing (delocalizing long-range interactions) and may be at the origin of a localization effect in driven systems. To capture this phenomenon it is crucial to

⁴ The last dipolar term $\propto \hat{S}_i^z \hat{S}_j^z$ in Eq. (2) is dropped as it commutes with all the operators \hat{S}_i^z .

go beyond the conventional weak-coupling secular approximation [16] and solve a more general GKSL equation [58–60]. In the context of DNP, our work provides an explanation for the breakdown of thermal mixing upon increasing the temperature of the sample. Its origin lies in the enhanced dynamics of the vibrational modes. In our model we used heuristic values of the microscopic timescales consistent with the experimental values of the standard T_1 and T_2 relaxation times. The present analysis calls for a thorough experimental test of the influence of temperature on the different regimes of hyperpolarization.

Acknowledgments – We thank Fabien Alet, Letícia Cugliandolo, Andrea De Luca, Laura Foini, Nicolas Laflorencie, Leonardo Mazza and Marco Schiró for valuable discussions around different facets of this work. We also are grateful to Filippo Vicentini for advices on the numerical methods. We acknowledge funding from the ANR-16-CE30-0023-01 (THERMOLOC) grant and the Galileo Galilei Institute for hospitality during part of this project.

Supplementary Material

In the supplementary material we provide some technical details and additional numerics. In Sec. I we review the derivation of the different master equations analyzed in the main text (secular, nonsecular and Hilbert master equations). In Sec. II we derive a numerically convenient formula to compute the EPR spectrum. In Sec. III we display additional plots of EPR and polarization profiles, for an ETH and a MBL Hamiltonian. We explain the fitting procedure introduced in [42] to a spin-temperature ansatz and exhibit extra data concerning the spectral properties of the bath-induced localized steady state. We also discuss the effect of the different bath timescales in the DNP model. The numerics are done for the $N = 10$ spins setup of the main text, but for completeness we analyze as well a case of full localization with $N = 12$ spins. Finally in Sec. V we explain the choice of our DNP Hamiltonian and show a simple model of coupling to the bath that allow to compute the microscopic bath timescales $T(|\omega|)$ as a function of frequency and temperature. These timescales are decreasing with temperature, an essential feature for the Zeno localization discussed in the main text.

CONTENTS

I. Open and driven system: Weak-coupling nonsecular master equation	7
A. Born-Markov approximation at weak coupling	7
B. Secular approximation and the Gorini-Kossakowski-Sudarshan-Lindblad equation	8
C. The nonsecular quantum master equation	9
1. Derivation of the nonsecular equation	9
2. Lamb shift and nonsecular jump operators	11
D. Turning the microwaves on	11
E. The Hilbert approximation	12
F. Comparison between secular and nonsecular GKSL equations	14
II. Electron Paramagnetic Resonance spectrum	14
III. Bath-induced localization by temperature variation: additional numerical results	16
A. Thermal mixing and spin temperature behavior	16
B. Estimating the spin-temperature ansatz parameters from simulation data	18
C. Hole burning	18
D. Spectral properties of the stationary state	20
IV. A toy model for Zeno localisation	22
V. Microscopic model of the electronic spins and bath	23
A. Coupling between spins and the magnetic field	23
B. Vibrational modes of the embedding material	24
1. Direct process	24
2. Two-phonon processes	24
3. Discussion of the one- and two-phonon bath timescales	25
References	26

I. OPEN AND DRIVEN SYSTEM: WEAK-COUPLED NONSECULAR MASTER EQUATION

The electronic spin system is in contact with a thermal reservoir and irradiated by microwaves. The total Hamiltonian reads

$$H_{\text{tot}} = H_{\text{S}} + H_{\text{MW}}(t) + H_{\text{int}} + H_{\text{B}} \quad (\text{S1})$$

In this section we will carefully study the system-bath interaction to derive an effective evolution of the spin system. We thus switch the microwaves off $H_{\text{MW}}(t) = 0$ and shall reinstate them in Sec. ID. The term H_{int} describes the coupling of the bath to the spins and H_{B} the Hamiltonian of the bath alone, assumed to remain in equilibrium at inverse temperature β . The system-bath interaction is written as

$$H_{\text{int}} = \sum_{\substack{i=1, \dots, N \\ \mu=x, y, z}} S_i^\mu \otimes B_i^\mu \quad (\text{S2})$$

where B_i^μ are Hermitian operators acting on the bath's Hilbert space, representing vibrational modes of the glassy medium. This choice shall be justified for diluted spins in Sec. V, where it also turns out the bath degrees of freedom can be considered *independent*:

$$\langle B_i^\mu(t) B_j^\nu(t') \rangle_B = 0 \quad \text{if } (i, \mu) \neq (j, \nu) \quad (\text{S3})$$

where $\langle \bullet \rangle_B = \text{Tr}(\bullet \rho_B)$ are bath averages with $\rho_B = e^{-\beta H_B} / \text{Tr} e^{-\beta H_B}$, and $B_i^\mu(t) = e^{itH_B} B_i^\mu e^{-itH_B}$. Besides the bath degrees of freedom are fluctuations that satisfy $\langle B_i^\mu \rangle_B = 0$.

In the following we first summarize the steps in [16, Sec.3.3] to treat perturbatively the effect of the bath on the system evolution. We then review the standard secular approximation that allow to turn this expansion into a Gorini-Kossakowski-Sudarshan-Lindblad master equation. Next we summarize the steps that provide a GKLS form without throwing away nonsecular terms, introduced in Ref. [58], by modifying the Markov approximation. Finally we show how to include the microwave drive in this approach and give the main formal difference between secular and nonsecular master equations that account for the effects analyzed in this article.

A. Born-Markov approximation at weak coupling

We start defining the non-interacting Hamiltonian $H_0 = H_{\text{S}} + H_{\text{B}}$ and the corresponding unitary evolution operator $U_0(t) = e^{-itH_0}$. The evolution of the whole system's density matrix is ruled by the Liouville-von Neumann equation which reads $\dot{\rho}_{\text{tot}} = -i[H, \rho_{\text{tot}}]$ in Schrödinger's picture. Since we treat H_{int} as a perturbation it is more convenient to start from the interaction picture version of it,

$$\dot{\rho}(t) = -i[\tilde{H}_{\text{int}}(t), \rho(t)] \quad (\text{S4})$$

where by definition $\rho(t) = U_0^\dagger(t) \rho_{\text{tot}}(t) U_0(t)$ and $\tilde{H}_{\text{int}}(t) = U_0^\dagger(t) H_{\text{int}} U_0(t)$.

We aim at getting an equation for the reduced density matrix describing the spin system $\rho_{\text{S}} = \text{Tr}_B \rho$. At weak coupling⁵ one (i) solves perturbatively Eq. (S4) by integrating it once, $\rho(t) = \rho(0) - i \int_0^t ds [\tilde{H}_{\text{int}}(s), \rho(s)]$, and plugging the solution back in Eq. (S4) – note that there is no approximation made in this step – (ii) makes the *Born approximation* $\rho(t) \simeq \rho_{\text{S}}(t) \otimes \rho_B$. One obtains after tracing over the bath

$$\dot{\rho}_{\text{S}}(t) = - \int_0^t ds \text{Tr}_B [\tilde{H}_{\text{int}}(t), [\tilde{H}_{\text{int}}(s), \rho_{\text{S}}(s) \otimes \rho_B]] \Big|_{\tau=t-s} - \int_0^t d\tau \text{Tr}_B [\tilde{H}_{\text{int}}(t), [\tilde{H}_{\text{int}}(t-\tau), \rho_{\text{S}}(t-\tau) \otimes \rho_B]] \quad (\text{S5})$$

The latter equation is not affected by the additional term coming from the initial condition when integrating Eq. (S4), as with $S_i^\mu(t) = e^{itH_{\text{S}}} S_i^\mu e^{-itH_{\text{S}}}$,

$$\text{Tr}_B [\tilde{H}_{\text{int}}(t), \rho(0)] = \sum_{i, \mu} [S_i^\mu(t), \rho_{\text{S}}(0)] \text{Tr}(B_i^\mu \rho_B) = 0 \quad (\text{S6})$$

The second approximation, after the weak coupling, is a *Markov approximation*:

$$\dot{\rho}_{\text{S}}(t) = - \int_0^\infty d\tau \text{Tr}_B [\tilde{H}_{\text{int}}(t), [\tilde{H}_{\text{int}}(t-\tau), \rho_{\text{S}}(t) \otimes \rho_B]] \quad (\text{S7})$$

The latter approximation amounts to say that products like $\tilde{H}_{\text{int}}(t) \tilde{H}_{\text{int}}(t-\tau)$ decay very rapidly to zero with τ compared to the relaxation time τ_R of the system (the relaxation time of $\rho_{\text{S}}(t)$), which is the case if the bath correlation functions (whose relaxation time is τ_B) decay very fast: $\tau_B \ll \tau_R$. The evolution is now Markovian. Note that there is not a unique way to perform this approximation, as there is a wide freedom in the choice of the time substitution made above $t - \tau \rightarrow t$: for instance any time t' such that $|(t - \tau) - t'| \lesssim \tau_B$ could be chosen.

⁵ It can be shown through the Nakajima-Zwanzig projection operator formalism [16, Sec.9.1] that Eq. (S5) is actually exact at second order in H_{int} (provided Eq. (S6)). Alternatively, a simpler cumulant expansion has been devised by Alicki and collaborators in [56, 57] for the evolution operator Λ such that

$\rho_{\text{S}}(t) = \text{Tr}_B \rho(t) = \Lambda(t, 0) \rho_{\text{S}}(0)$. Taking the time derivative of the latter equation, one recovers the same result at second order in H_{int} . This result is guessed in the present perturbative self-consistent derivation.

B. Secular approximation and the Gorini-Kossakowski-Sudarshan-Lindblad equation

We shall now see that Eq. (S7) can be simplified further⁶ using the eigendecomposition of H_S . We define the projector $\Pi(\varepsilon)$ on the eigenspace associated to the energy ε of H_S , and for each gap ω of the spin Hamiltonian

$$S_i^\mu(\omega) \equiv \sum_{\varepsilon' - \varepsilon = \omega} \Pi(\varepsilon) S_i^\mu \Pi(\varepsilon') \quad \Rightarrow \quad H_{\text{int}} = \sum_{i, \mu, \omega} S_i^\mu(\omega) \otimes B_i^\mu \quad (\text{S10})$$

This allows to simply write

$$\tilde{H}_{\text{int}}(t) = \sum_{i, \mu, \omega} e^{-i\omega t} S_i^\mu(\omega) \otimes B_i^\mu(t) = \sum_{i, \mu, \omega} e^{i\omega t} S_i^\mu(\omega)^\dagger \otimes B_i^{\mu\dagger}(t) \quad (\text{S11})$$

with $S_i^\mu(\omega)^\dagger = S_i^\mu(-\omega)$ from Eq. (S10). Plugging it in Eq. (S7) using the Hermitian conjugated form for $\tilde{H}_{\text{int}}(t)$ and the direct one for $\tilde{H}_{\text{int}}(t - \tau)$, we get

$$\dot{\rho}_S(t) = \sum_{\substack{i, j \\ \mu, \nu}} \sum_{\omega, \omega'} \Gamma_{ij}^{\mu\nu}(\omega) e^{i(\omega' - \omega)t} \left(S_j^\nu(\omega) \rho_S(t) S_i^\mu(\omega')^\dagger - S_i^\mu(\omega')^\dagger S_j^\nu(\omega) \rho_S(t) \right) + \text{H.c.} \quad (\text{S12})$$

The equilibrium bath correlation functions $\Gamma_{ij}^{\mu\nu}(\omega)$ satisfy time-translational invariance owing to the commutation $[H_B, \rho_B] = 0$, so that using $\langle B_i^\mu(t) B_j^\nu(t - \tau) \rangle = \langle B_i^\mu(\tau) B_j^\nu(0) \rangle$, they are defined as

$$\Gamma_{ij}^{\mu\nu}(\omega) = \int_0^\infty d\tau e^{i\omega\tau} \langle B_i^\mu(\tau) B_j^\nu(0) \rangle_B = \delta_{ij} \delta_{\mu\nu} \Gamma(\omega) \quad (\text{S13})$$

We assumed as previously mentioned that different degrees of freedom of the bath decouple. Let us then write Eq.(S12) back to the Schrödinger picture (see Eq. (S8)):

$$\dot{\rho}_S^s(t) = -i [H_S, \rho_S^s(t)] + \sum_{i, \mu} \sum_{\omega, \omega'} \left\{ \Gamma(\omega) \left(S_i^\mu(\omega) \rho_S^s(t) S_i^\mu(\omega')^\dagger - S_i^\mu(\omega')^\dagger S_i^\mu(\omega) \rho_S^s(t) \right) + \text{H.c.} \right\} \quad (\text{S14})$$

where we note that the phases disappear compared to the Heisenberg picture equation (S12). Eq.(S14) is written using an eigenbasis of H_S . This is a convenient choice, but we could have chosen a different basis, yielding a more complicated equation, and at this level of approximation the time evolution of ρ_S^s would be identical.

Nonetheless our Markovian quantum master equation must preserve the defining properties of a density matrix (such as positivity and trace), *i.e.* be of the Gorini-Kossakowski-Sudarshan-Lindblad (GKSL) form $\dot{\rho} = \mathcal{L}\rho$ where the superoperator \mathcal{L} is a generator of a quantum dynamical semi-group [16, Sec.3.2]. A more explicit definition is given by Eq. (4) of the main text. This is not guaranteed by Eq. (S14). To ensure so in this weak-coupling approach, the standard prediction resorts to the *secular approximation*. It amounts to neglect the terms for which $\omega \neq \omega'$. It is then useful to define the real and imaginary parts:

$$\begin{aligned} \Gamma(\omega) &= \frac{\gamma(\omega)}{2} + iS(\omega), \quad S(\omega) = \text{Im } \Gamma(\omega) \\ \gamma(\omega) &= 2\text{Re } \Gamma(\omega) = \int_{-\infty}^\infty d\tau e^{i\omega\tau} \langle B_i^\mu(\tau) B_i^\mu(0) \rangle_B \end{aligned} \quad (\text{S15})$$

As ρ_B describes the Boltzmann-Gibbs distribution at inverse temperature β , one can easily prove the Kubo-Martin-Schwinger condition $\langle B_i^{\mu\dagger}(t) B_j^\nu(0) \rangle_B = \langle B_j^\nu(0) B_i^{\mu\dagger}(t + i\beta) \rangle_B$, from which the detailed balance condition $\gamma(\omega)/\gamma(-\omega) = e^{\beta\omega}$ follows [64, Sec.12]. We can thus equivalently define

$$\gamma(\omega) = \frac{h(\omega)}{T(|\omega|)} \quad \text{with} \quad h(\omega) = \frac{e^{\beta\omega}}{1 + e^{\beta\omega}} \quad (\text{S16})$$

⁶ Let us note $\rho_S^s = \text{Tr}_B \rho_{\text{tot}}$ the Schrödinger picture density matrix. We have

$$\begin{aligned} \rho_S(t) &= \text{Tr}_B \left(U_0^\dagger(t) \rho_{\text{tot}}(t) U_0(t) \right) \\ &= e^{itH_S} \text{Tr}_B \left(e^{itH_B} \rho_{\text{tot}}(t) e^{-itH_B} \right) e^{-itH_S} \\ &= e^{itH_S} \rho_S^s(t) e^{-itH_S} \end{aligned} \quad (\text{S8})$$

i.e. the standard relationship between Heisenberg and Schrödinger pictures for the reduced system S. If we switch to the Schrödinger picture, Eq. (S7) becomes

$$\begin{aligned} \dot{\rho}_S^s(t) &= -i [H_S, \rho_S^s(t)] \\ &+ \sum_{\substack{i, j \\ \mu, \nu}} \int_0^\infty d\tau \left(S_j^\nu(-\tau) \rho_S^s(t) S_i^\mu - S_i^\mu S_j^\nu(-\tau) \rho_S^s(t) \right) \langle B_i^\mu(\tau) B_j^\nu \rangle_B \\ &+ \text{H.c.} \end{aligned} \quad (\text{S9})$$

We used time-translation invariance of the equilibrium bath correlation function. One sees that the extra difficulty of evolving in time the interaction Hamiltonian remains even in this formulation, which calls for the eigendecomposition of H_S .

$T(|\omega|)$ defines relaxation times of the system for transitions at energy ω while h enforces the detailed balance condition. Inserting the above definitions in Eq. (S14) where the $\omega \neq \omega'$ terms are neglected, one arrives at a GKSL master equation:

$$\begin{aligned}\dot{\rho}_S^s(t) &= -i [H_S + H_{LS}, \rho_S^s(t)] + \mathcal{D}\rho_S^s(t) \\ H_{LS} &= \sum_{i,\mu,\omega} S(\omega) S_i^{\mu\dagger}(\omega) S_i^\mu(\omega) \\ \mathcal{D}\rho &= \sum_{i,\mu,\omega} \frac{h(\omega)}{T(|\omega|)} \left(S_i^\mu(\omega) \rho S_i^{\mu\dagger}(\omega) - \frac{1}{2} \{ S_i^{\mu\dagger}(\omega) S_i^\mu(\omega), \rho \} \right)\end{aligned}\quad (\text{S17})$$

The *Lamb-shift* Hamiltonian H_{LS} being Hermitian and $[H_S, H_{LS}] = 0$, it can be absorbed into the system Hamiltonian H_S in Eq. (S17) just by shifting the energy levels.

For our many-body electron system described by the Hamiltonian H_S , it is safe to consider the energy gaps as non degenerate. Eq. (S17) takes then a simple form in the eigenbasis $\{|n\rangle\}$

$$\begin{aligned}\dot{\rho}_{nn} &= \sum_{m \neq n} W_{mn}^B \rho_{mm} - W_{nm}^B \rho_{nn} \\ \dot{\rho}_{m \neq n} &= - \left(i\omega_{mn} + \frac{1}{T_{mn}} \right) \rho_{m \neq n}\end{aligned}\quad (\text{S18})$$

with respectively the bath and decoherence rates

$$\begin{aligned}W_{nm}^B &= \frac{h(\omega_{nm})}{T(|\omega_{nm}|)} \sum_{i,\mu} |\langle n | S_i^\mu | m \rangle|^2 \\ \frac{1}{T_{nm}} &= \frac{1}{2} \sum_{k \neq n} h(\omega_{nk}) W_{nk}^B + \frac{1}{2} \sum_{k \neq m} h(\omega_{mk}) W_{mk}^B + \frac{1}{4T(0)} \sum_i \langle n | S_i^z | n \rangle^2 + \langle m | S_i^z | m \rangle^2 - 2 \langle n | S_i^z | n \rangle \langle m | S_i^z | m \rangle\end{aligned}\quad (\text{S19})$$

The first line in Eq. (S18) is a master equation for the diagonal elements only, with rates satisfying the detailed balance condition $W_{mn}^B/W_{nm}^B = e^{\beta\omega_{mn}}$, and $\omega_{mn} = \varepsilon_m - \varepsilon_n$ the gap between levels m and n of the Hamiltonian $H_S + H_{LS}$. The second equation describes the evolution of the off-diagonal terms: the first term $i\omega_{mn}$ represents the dephasing from the unitary evolution while the second term T_{mn}^{-1} describes the decoherence due to the bath. Under this evolution, the coherences vanish exponentially while the populations tend to their thermal values imposed by the Boltzmann distribution, emerging from the detailed balance at temperature β^{-1} .

Note that *after* the secular approximation, the time evolution of ρ_S^s depends on the choice of the eigenbasis. In presence of a drive, different steady states can be reached by changing this choice of basis, which is an inconsistency of the secular approximation.

C. The nonsecular quantum master equation

A usual justification [16] for the secular approximation, on top of allowing to preserve the properties of a density matrix, is that in Heisenberg representation the terms $\omega \neq \omega'$ produce rapidly oscillating phases (see Eq. (S12)) which cancel. Yet for a large many-body system there exist a lot of quasi-degenerate gaps for which the argument does not hold. There is a way to retain all the terms from Eq. (S12) while ensuring a GKSL form by modifying the Markovian approximation. Below we summarize the derivation as given by Nathan and Rudner's recent paper [58].

1. Derivation of the nonsecular equation

We start back from Eqs. (S5)-(S7). Coming back to the variable s we see that the initial condition is in the end prepone to $-\infty$ by the Markov approximation performed there, and we have

$$\dot{\rho}_S(t) = - \int_{-\infty}^t ds \text{Tr}_B \left[\tilde{H}_{\text{int}}(t), [\tilde{H}_{\text{int}}(s), \rho_S(t) \otimes \rho_B] \right] = - \sum_{i,\mu} \int_{-\infty}^t dt' \Gamma(t-t') [S_i^\mu(t), S_i^\mu(t') \rho_S(t)] + \text{H.c.} \quad (\text{S20})$$

A first progress is to take the square root of the bath rate in Fourier space, *i.e.* to define g such that

$$\Gamma(t-t') = \int_{\mathbb{R}} ds g(t-s) g(s-t') \quad (\text{S21})$$

Eq. (S20) becomes

$$\begin{aligned}\dot{\rho}_S(t) &= \int_{\mathbb{R}^2} dt' ds \mathcal{F}(t, s, t') [\rho_S(t)] \\ \mathcal{F}(t, s, t') [\rho] &= \sum_{i,\mu} \theta(t-t') g(t-s) g(s-t') [S_i^\mu(t), S_i^\mu(t') \rho] + \text{H.c.}\end{aligned}\quad (\text{S22})$$

Integrating on $[t_1, t_2]$ with $t_2 - t_1 \gg \tau_B$:

$$\rho_S(t_2) - \rho_S(t_1) = \int_{t_1}^{t_2} dt \int_{\mathbb{R}^2} dt' ds \mathcal{F}(t, s, t')[\rho_S(t)] \quad (\text{S23})$$

Next, due to $t_2 - t_1 \gg \tau_B$, most contributions in the integrals of Eq. (S23) arise for $(t, s, t') \in [t_1, t_2]^3$, thus they are approximately unaffected if we change the boundaries as $\{-\infty < s, t' < \infty, t_1 \leq t \leq t_2\} \rightarrow \{-\infty < t, t' < \infty, t_1 \leq s \leq t_2\}$:

$$\rho_S(t_2) - \rho_S(t_1) \simeq \int_{t_1}^{t_2} ds \int_{\mathbb{R}^2} dt dt' \mathcal{F}(t, s, t')[\rho_S(s)] \quad (\text{S24})$$

where, similarly to Eq. (S7) one makes another Markovian type of approximation for the density matrix time dependence. Then we derive Eq. (S24) with respect to t_2 and set $t = t_2$:

$$\dot{\rho}_S(t) = \mathcal{L}(t)[\rho_S(t)] , \quad \mathcal{L}(t) = \int_{\mathbb{R}^2} ds ds' \mathcal{F}(s, t, s') \quad (\text{S25})$$

and using $\theta(t) = 1/2 + \text{sign}(t)/2$ helps us to disentangle the Lamb-shift and the jump operators:

$$\begin{aligned} \dot{\rho}_S(t) &= -i [H_{\text{LS}}(t), \rho_S(t)] + \sum_{i,\mu} A_i^\mu(t) \rho_S(t) A_i^\mu(t)^\dagger - \frac{1}{2} \left\{ A_i^\mu(t)^\dagger A_i^\mu(t), \rho_S(t) \right\} \\ A_i^\mu(t) &= \int_{\mathbb{R}} ds g(t-s) S_i^\mu(s) , \quad H_{\text{LS}}(t) = \frac{1}{2i} \sum_{i,\mu} \int_{\mathbb{R}^2} ds ds' S_i^\mu(s) g(t-s) g(t-s') S_i^\mu(s') \text{sign}(s-s') \end{aligned} \quad (\text{S26})$$

By Fourier transform and the definition (S21) we can relate $g(t)$ and $\gamma(\omega)$:

$$\tilde{g}(\omega) = \int_{\mathbb{R}} \frac{dt}{2\pi} e^{i\omega t} g(t) \Rightarrow \tilde{g}(\omega) = \frac{\sqrt{\gamma(\omega)}}{2\pi} \quad (\text{S27})$$

We now seek to come back to Schrödinger representation and decompose the operators on the eigenbasis of the spin Hamiltonian through $S_i^\mu(t) = \sum_{\omega} S_i^\mu(\omega) e^{-i\omega t}$. For the Lamb-shift Hamiltonian we show through the Fourier decompositions

$$\begin{aligned} H_{\text{LS}}(t) &= \sum_{i,\mu,\omega,\omega'} S_i^\mu(\omega) S_i^\mu(\omega') e^{-it(\omega+\omega')} \int_{\mathbb{R}^2} d\Omega d\Omega' \tilde{g}(\Omega) \tilde{g}(\Omega') k(\omega + \Omega, \omega' - \Omega') \\ k(p, q) &= \frac{1}{2i} \int_{\mathbb{R}^2} ds ds' \text{sign}(s-s') e^{-i(p s + q s')} \end{aligned} \quad (\text{S28})$$

Through a direct computation and usual regularizations we get

$$k(p, q) = 2\pi\delta(p+q) \text{Im} \frac{1}{ip+0^+} \quad (\text{S29})$$

which yields

$$H_{\text{LS}}(t) = \sum_{i,\mu,\omega,\omega'} S_i^\mu(\omega) S_i^\mu(\omega') e^{-it(\omega+\omega')} 2\pi\mathcal{P} \int_{\mathbb{R}} d\Omega \frac{\tilde{g}(\Omega - \omega) \tilde{g}(\Omega + \omega')}{\Omega} \quad (\text{S30})$$

where \mathcal{P} stands for Cauchy's principal value. It is then straightforward to pass from Heisenberg to Schrödinger representations, which cancels the phases. This allows to define nonsecular jump operators

$$A_i^\mu = \sum_{\omega} \sqrt{\gamma(\omega)} S_i^\mu(\omega) \quad (\text{S31})$$

In Schrödinger representation, the nonsecular version of Eq. (S17) thus reads:

$$\begin{aligned} \dot{\rho}_S^s(t) &= -i [H_S + H_{\text{LS}}, \rho_S^s(t)] + \sum_{i,\mu} A_i^\mu \rho_S^s(t) A_i^{\mu\dagger} - \frac{1}{2} \left\{ A_i^{\mu\dagger} A_i^\mu, \rho_S^s(t) \right\} \\ H_{\text{LS}} &= \sum_{i,\mu,\omega,\omega'} S_i^\mu(\omega) S_i^\mu(\omega') f(\omega, \omega') , \quad f(\omega, \omega') = \mathcal{P} \int_{\mathbb{R}} \frac{d\Omega}{2\pi} \frac{\sqrt{\gamma(\Omega - \omega) \gamma(\Omega + \omega')}}{\Omega} \end{aligned} \quad (\text{S32})$$

The Lamb-shift H_{LS} is Hermitian and the evolution is thus manifestly in GKSL form. The secular equation is recovered again by throwing away all gaps $\omega \neq \omega'$ in the sums.

2. Lamb shift and nonsecular jump operators

For our system the Lamb-shift H_{LS} becomes negligible due to the wide difference of characteristic energy scales. Indeed considering that $f(\omega, \omega')$ is smooth in both arguments, $f(\omega, \omega') \simeq f(0, 0)$ for S_i^z gaps while for $S_i^{x,y}$ we can use $S_i^\pm = S_i^x \pm iS_i^y$ operators and get:

$$\begin{aligned}
H_{\text{LS}} &\simeq f(0, 0) \sum_i (S_i^z)^2 + \sum_{i, \omega, \omega'} \frac{1}{4} (S_i^+(\omega) + S_i^-(\omega)) (S_i^+(\omega') + S_i^-(\omega')) f(\omega, \omega') \\
&\quad - \sum_{i, \omega, \omega'} \frac{1}{4} (S_i^-(\omega) - S_i^+(\omega)) (S_i^-(\omega') - S_i^+(\omega')) f(\omega, \omega') \\
&= \frac{N}{4} f(0, 0) + \frac{1}{2} \sum_{i, \omega, \omega'} f(\omega, \omega') [S_i^+(\omega) S_i^-(\omega') + S_i^-(\omega) S_i^+(\omega')] \\
&\simeq \frac{N}{4} f(0, 0) + \frac{1}{2} \sum_{i, \omega, \omega'} [f(-\omega_e, \omega_e) S_i^+(\omega) S_i^-(\omega') + f(\omega_e, -\omega_e) S_i^-(\omega) S_i^+(\omega')] \\
&= \frac{N}{4} f(0, 0) + \frac{f(\omega_e, -\omega_e)}{2} \sum_i (S_i^+ S_i^- + S_i^- S_i^+) = \frac{N}{4} (f(0, 0) + 2f(\omega_e, -\omega_e)) \mathbb{1}
\end{aligned} \tag{S33}$$

where we have used the symmetry $f(\omega_e, -\omega_e) = f(-\omega_e, \omega_e)$. In conclusion the Lamb-shift Hamiltonian is proportional to the identity up to very small corrections and thus we can take $[H_{\text{LS}}, \rho_S^s(t)] = 0$ in Eq. (S32).

With very similar considerations one obtains from the definition (S31) the form of the nonsecular jump operators given by Eq. (7) of the main text.

D. Turning the microwaves on

In the following we set $H_{\text{LS}} = 0$ and incorporate the microwave field⁷

$$H_{\text{MW}}(t) = \omega_1 [S^x \cos(\omega_{\text{MW}} t) + S^y \sin(\omega_{\text{MW}} t)] \tag{S34}$$

The interaction picture dynamics Eq. (S4) becomes

$$\dot{\rho}(t) = -i[\tilde{H}_{\text{MW}}(t), \rho(t)] - i[\tilde{H}_{\text{int}}(t), \rho(t)] \tag{S35}$$

with $\tilde{H}_{\text{MW}}(t) = U_0^\dagger(t) H_{\text{MW}}(t) U_0(t) = e^{iH_{\text{S}} t} H_{\text{MW}}(t) e^{-iH_{\text{S}} t}$. Then we treat the last term as before by integrating once the equation and obtain

$$\dot{\rho}(t) = -i[\tilde{H}_{\text{MW}}(t), \rho(t)] - \int_0^t ds [\tilde{H}_{\text{int}}(t), [\tilde{H}_{\text{int}}(s), \rho(s)]] - \int_0^t ds [\tilde{H}_{\text{int}}(t), [\tilde{H}_{\text{MW}}(s), \rho(s)]] - i[\tilde{H}_{\text{int}}(t), \rho(0)] \tag{S36}$$

Then if we make the Born approximation $\rho(t) \simeq \rho_S(t) \otimes \rho_B$ and trace over the bath, since $\tilde{H}_{\text{MW}}(s)$ acts only on the spin degrees of freedom, the last two terms in Eq. (S36) are zero if the bath degrees of freedom are of average zero, $\langle B_i^\mu(t) \rangle_B = 0$. Then the quadratic term in H_{int} can be dealt with as in the previous sections.

In Schrödinger picture we therefore get the equation, similar to Eq. (S32):

$$\begin{aligned}
\dot{\rho}_S^s(t) &= -i[H_{\text{MW}}(t), \rho_S^s(t)] - i[H_S, \rho_S^s(t)] + \mathcal{D}\rho_S^s(t) \\
\mathcal{D}\rho &= -i[H_{\text{LS}}, \rho] + \sum_{i, \mu} A_i^\mu \rho A_i^{\mu\dagger} - \frac{1}{2} \left\{ A_i^{\mu\dagger} A_i^\mu, \rho \right\}
\end{aligned} \tag{S37}$$

Note that $H_{\text{MW}}(t)$ is time dependent ; a usual trick for NMR studies is to place ourselves in a rotated frame given by the Larmor precession [65]. We shall now rotate accordingly the reference frame, which, if done at frequency ω_{MW} , makes the microwaves field effectively stationary, resulting in a time-independent dynamical semigroup generator for Eq. (S37). The rotation is implemented as

$$U_{\text{MW}}(t) = e^{-i\omega_{\text{MW}} t S^z}, \quad \rho_r(t) = U_{\text{MW}}^\dagger(t) \rho_S^s(t) U_{\text{MW}}(t) \tag{S38}$$

Since $[S^z, H_S] = 0$, the unperturbed spin Hamiltonian is unchanged. We then need to express the rotated microwave Hamiltonian $U_{\text{MW}}^\dagger(t) H_{\text{MW}}(t) U_{\text{MW}}(t)$. To achieve this one can write the microwave Hamiltonian as

$$H_{\text{MW}}(t) = \frac{\omega_1}{2} (S^- e^{i\omega_{\text{MW}} t} + S^+ e^{-i\omega_{\text{MW}} t}) \tag{S39}$$

⁷ If the field is oscillating along a single direction, e.g. $H_{\text{MW}}(t) = \omega_1 S^x \cos(\omega_{\text{MW}} t)$, the conclusion of this section re-

mains valid at small drive through the rotating wave approximation [41, 42].

and we define $S^\pm(t) = U_{\text{MW}}^\dagger(t)S^\pm U_{\text{MW}}(t)$ verifying

$$\dot{S}^\pm(t) = U_{\text{MW}}^\dagger(t)i\omega_{\text{MW}} [S^z, S^\pm] U_{\text{MW}}(t) = \pm i\omega_{\text{MW}} S^\pm(t) \quad \Rightarrow \quad S^\pm(t) = e^{\pm i\omega_{\text{MW}} t} S^\pm \quad (\text{S40})$$

where we used $[S^z, S^\pm] = \pm S^\pm$. We thus conclude that in the rotating frame the microwave Hamiltonian becomes stationary:

$$U_{\text{MW}}^\dagger(t)H_{\text{MW}}(t)U_{\text{MW}}(t) = \omega_1 S^x \quad (\text{S41})$$

and the GKSL equation (S37) becomes

$$\dot{\rho}_r(t) = -i [H_{\text{S}} + \omega_1 S^x - \omega_{\text{MW}} S^z, \rho_r(t)] + U_{\text{MW}}^\dagger(t)\mathcal{D}\left(U_{\text{MW}}(t)\rho_r(t)U_{\text{MW}}^\dagger(t)\right)U_{\text{MW}}(t) \quad (\text{S42})$$

Let us define as before $H_{\text{S}}|n\rangle = \varepsilon_n|n\rangle$ the eigendecomposition. As $[S^z, H_{\text{S}}] = 0$, the total polarization along z is conserved, and we note $S^z|n\rangle = s_n^z|n\rangle$. We consider as well for large enough N that the finite gaps $\omega_{nm} = \varepsilon_n - \varepsilon_m$ are non degenerate, implying that the jump operators read:

$$S_i^z(0) = \sum_n \langle n| S_i^z |n\rangle |n\rangle\langle n|, \quad S_i^\mu(\omega_{nm}) = |m\rangle\langle m| S_i^\mu |n\rangle\langle n| \quad (\text{S43})$$

To analyze the last term of Eq. (S42), let us go back to the original dissipative part of Eq. (S37) (second line). It consists in sums over pairs of gaps (ω, ω') of the jumps operators (S43). Each term in this sum contains a product of the form

$$\langle n| S_i^\mu(\omega = \omega_{mn}) |m\rangle \langle m'| S_i^\mu(\omega' = \omega_{m'n'})^\dagger |n'\rangle \quad (\text{S44})$$

The bath operators are of two kinds: S_i^x, S_i^y which induce flips of the spin i with energy jump $\approx \pm\omega_e$ and S_i^z whose transitions have gaps $\omega \ll \omega_e$ which conserve the total polarization along z . For the S_i^x, S_i^y operators, there are 4 possibilities:

- $\omega \approx \omega_e$ and $\omega' \approx -\omega_e$: both factors imply a flip $|-\rangle_i \rightarrow |+\rangle_i$, so that $i\langle n| S_i^x |m\rangle = \langle n| S_i^y |m\rangle$ and $i\langle m'| S_i^x |n'\rangle = \langle m'| S_i^y |n'\rangle$. Consequently the terms generated by the operator S_i^y have the opposite value to the one generated by S_i^x : and their contribution vanishes.
- $\omega \approx -\omega_e$ and $\omega' \approx \omega_e$: both factors imply a flip $|+\rangle_i \rightarrow |-\rangle_i$, so that $-i\langle n| S_i^x |m\rangle = \langle n| S_i^y |m\rangle$ and $-i\langle m'| S_i^x |n'\rangle = \langle m'| S_i^y |n'\rangle$. Once again their combined contribution vanishes.
- $\omega \approx \omega'(\approx \pm\omega_e)$: contrary to the above cases those terms are allowed.

For all allowed transitions the total polarization jump for the term (S44) (*i.e.* from $|n\rangle$ to $|n'\rangle$) is $s_n^z - s_m^z - (s_{n'}^z - s_{m'}^z) = 0$. This holds for the S_i^x, S_i^y operators (for which $s_n^z - s_m^z = s_{n'}^z - s_{m'}^z = \pm 1$), but also for S_i^z transitions where $s_n^z = s_m^z$ and $s_{n'}^z = s_{m'}^z$.

When shifting to the rotating frame, the rotation (S38) produces oscillating phases in the dissipative term of Eq. (S42) according to the following relation

$$U_{\text{MW}}(t)S_i^\mu(\omega_{mn})U_{\text{MW}}^\dagger(t) = e^{i\omega_{\text{MW}} t(s_n^z - s_m^z)} S_i^\mu(\omega_{mn}) \quad (\text{S45})$$

Therefore each term writing as Eq. (S44) receives a phase $e^{i\omega_{\text{MW}} t[s_n^z - s_m^z - (s_{n'}^z - s_{m'}^z)]}$. As emphasized above, this phase is 1 for all allowed transitions. Consequently $U_{\text{MW}}^\dagger(t)\mathcal{D}\left(U_{\text{MW}}(t)\rho_r(t)U_{\text{MW}}^\dagger(t)\right)U_{\text{MW}}(t) = \mathcal{D}\rho_r(t)$, *i.e.* the quantum master equation in the rotating frame is

$$\dot{\rho}_r(t) = -i [H_{\text{S}} + H_{\text{LS}} + \omega_1 S^x - \omega_{\text{MW}} S^z, \rho_r(t)] + \sum_{i,\mu} A_i^\mu \rho_r(t) A_i^{\mu\dagger} - \frac{1}{2} \left\{ A_i^{\mu\dagger} A_i^\mu, \rho_r(t) \right\} \quad (\text{S46})$$

Note that if for example only the spin j is irradiated, one has to replace $S^x \rightarrow S_j^x$.

E. The Hilbert approximation

In this section we provide the details of the Hilbert approximation for the secular GKSL equation given by Eq. (S46) where nonsecular terms $\omega \neq \omega'$ are thrown away (as in Eq. (S17)), which amounts to take $A_i^\mu \rightarrow \sqrt{\gamma(\omega)} S_i^\mu(\omega)$ in Eq. (S46). Below we drop the rotating frame index r and consider $H_{\text{LS}} = 0$ as explained in the previous sections:

$$\dot{\rho} = -i[H_{\text{S}} - \omega_{\text{MW}} S^z + \omega_1 S^x, \rho] + \sum_{\omega, i, \mu} \frac{h(\omega)}{T(|\omega|)} \left(S_i^\mu(\omega) \rho S_i^\mu(\omega)^\dagger - \frac{1}{2} \left\{ S_i^\mu(\omega)^\dagger S_i^\mu(\omega), \rho \right\} \right) \quad (\text{S47})$$

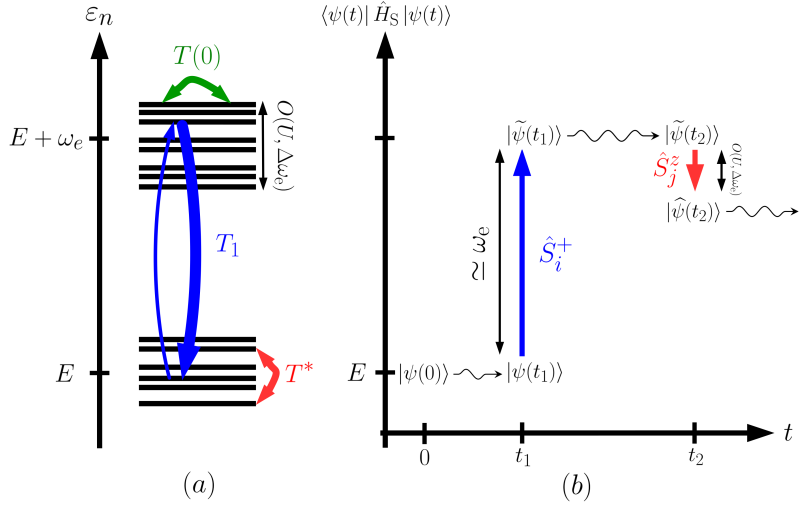


FIG. S5. Effective quantum dynamics of the electron spins. (a) Energy levels of H_S are drawn. They are arranged into $N+1$ polarization sectors, each containing many levels, separated by multiples of ω_e . In the Hilbert approximation due to fast dephasing, the jump operators (arrows) select transitions between eigenstates with corresponding timescales, and the system is a mixture of H_S eigenstates. (b) Example of a nonsecular quantum trajectory in its average energy vs time plane: the unitary dynamics (wavy arrows) gets projected with a characteristic rate by spatially-localized jump operators. The Hilbert approximation is retrieved for slow jump rates for which the unitary evolution is able to project the system onto eigenstates.

Projecting on the diagonal and off-diagonal terms ($n \neq m$) leads to

$$\begin{aligned} \dot{\rho}_{nn} &= \sum_{k \neq n} W_{kn}^B \rho_{kk} - W_{nk}^B \rho_{nn} - i\omega_1 (\langle n | S^x | k \rangle \rho_{kn} - \text{c.c.}) \\ \dot{\rho}_{nm} &= - \left(i\Delta\omega_{nm} + \frac{1}{T_{nm}} \right) \rho_{nm} - i\omega_1 \sum_k (\langle n | S^x | k \rangle \rho_{km} - \langle k | S^x | m \rangle \rho_{nk}) \end{aligned} \quad (\text{S48})$$

where rates have been defined in Eq. (S19) and the dephasing is now

$$\Delta\omega_{nm} = \varepsilon_n - \varepsilon_m - (s_n^z - s_m^z) \omega_{\text{MW}} \quad (\text{S49})$$

If the term $i\Delta\omega_{nm} + 1/T_{nm}$ dominates the coherences' evolution – making them vanish exponentially fast – the dynamics is projected on the diagonal elements. This is the spirit of the *Hilbert approximation*. It is achieved by considering T_{nm} and $1/\Delta\omega_{nm}$ go to zero with $\Delta\omega_{nm} T_{nm}$ constant and solving perturbatively the master equation. We thus write the evolution as $\dot{\rho} = L_0 \rho + L_1 \rho$ with L_0 the dominant contribution to the generator, defined by

$$L_0 e_{nm} = \begin{cases} 0 & n = m \\ - \left(i\Delta\omega_{nm} + \frac{1}{T_{nm}} \right) e_{nm} & n \neq m \end{cases} \quad (\text{S50})$$

with $\{e_{nm}\}$ a basis for our $2^N \times 2^N$ density matrices: $(e_{nm})_{ab} = \delta_{an} \delta_{bm}$. At dominant order the steady-state density matrices fall in the subspace of diagonal matrices. Treating L_1 as a perturbation, the Hilbert approximation projects the dynamical evolution in the diagonal subspace, leading to an approximate master equation for the populations. Details of the (Schrieffer-Wolff) perturbation theory are described in [41, 66, 67]. One has to go to second order in L_1 to get the first terms dependent on $\Delta\omega_{nm}$ and T_{nm} . One finds the master equation for the populations

$$\dot{\rho}_{nn} = \sum_{n'} \left[(L_1)_{nn, n'n'} + \sum_{m \neq m'} \frac{(L_1)_{nn, mm'} (L_1)_{mm', n'n'}}{i\Delta\omega_{mm'} + 1/T_{mm'}} \right] \rho_{n'n'} \quad (\text{S51})$$

with the basis decomposition $(L_1 \rho)_{nm} = \sum_{ij} (L_1)_{nm, ij} \rho_{ij}$. Concretely the Hilbert rate equation (S51) reads in the present secular case

$$\dot{\rho}_{nn} = \sum_{m \neq n} \left[W_{mn}^B + W_{nm}^{\text{MW}} \right] \rho_{mm} - \left[W_{nm}^B + W_{nm}^{\text{MW}} \right] \rho_{nn} \quad (\text{S52})$$

where the microwave rates are

$$W_{nm}^{\text{MW}} = \frac{2\omega_1^2 T_{nm}}{1 + (T_{nm} \Delta\omega_{nm})^2} |\langle n | S^x | m \rangle|^2 \quad (\text{S53})$$

The physical interpretation of Hilbert versus nonsecular dynamics is sketched in Fig. S5.

F. Comparison between secular and nonsecular GKSL equations

In this section we highlight the additional terms contained in the nonsecular GKSL equation (S46) compared to the secular one (S47) (with $H_{\text{LS}} = 0$). We write the off-diagonal elements of the nonsecular equation in the eigenbasis, as these contain the main new terms to account for the bath-induced localization. The first line of each equation corresponds to the secular part given in Eq. (S48).

$$\begin{aligned} \dot{\rho}_{nm} = & - \left(i\Delta\omega_{nm} + \frac{1}{T_{nm}} \right) \rho_{nm} - i\omega_1 \sum_k (\langle n | S^x | k \rangle \rho_{km} - \langle k | S^x | m \rangle \rho_{nk}) \\ & + \sum_{\mu=x,y,z} \left[\sum_{\substack{k \neq n \\ k' \neq m}} \sqrt{\gamma(\omega_{kn})\gamma(\omega_{k'm})} \underbrace{\langle n | S_i^\mu | k \rangle}_{\omega=\omega_{kn}} \rho_{kk'} \underbrace{\langle k' | S_i^\mu | m \rangle}_{\omega'=\omega_{k'm}} - \frac{1}{2} \sum_{\substack{k \\ k' \neq n}} \sqrt{\gamma(\omega_{nk})\gamma(\omega_{k'k})} \underbrace{\langle n | S_i^\mu | k \rangle \langle k | S_i^\mu | k' \rangle}_{\omega'=\omega_{nk}, \omega=\omega_{k'k}} \rho_{k'm} \right. \\ & \left. - \frac{1}{2} \sum_{\substack{k \\ k' \neq m}} \sqrt{\gamma(\omega_{k'k})\gamma(\omega_{mk})} \rho_{nk'} \underbrace{\langle k' | S_i^\mu | k \rangle \langle k | S_i^\mu | m \rangle}_{\omega'=\omega_{k'k}, \omega=\omega_{mk}} \right] \end{aligned} \quad (\text{S54})$$

Some remarks:

1. The constraints over eigenstates indices below the sum signs correspond to secular terms already taken into account in the first line of the equation. For instance if the constraint is $k \neq n$ this means that the same term with $k = n$ is a secular term contained in the first line.
2. For $S_i^{x,y}$ terms, we have explicitly written the pair of gaps (ω, ω') involved. This emphasizes, as remarked in Sec. 1D, that terms not satisfying $\omega \approx \omega'$ actually vanish, although we have not mentioned it in the sums to lighten the notation. This is not true for S_i^z terms.
3. In the secular equation at small drive allows only a steady-state solution where all coherences $\rho_{nm} = 0$. The nonsecular terms render possible non-zero coherences in the stationary state: the system does not get projected anymore onto the Hamiltonian eigenstates. This can occur if timescale T^* gets lowered so that the nonsecular terms in Eq. (S54) do have an impact. This timescale comes from S_i^z transitions. All nonsecular S_i^z transitions in Eq. (S54) occur between different eigenstates ; as a consequence, in the limit of strong disorder or non-interacting spins, such terms vanish. This explains why the drastic effect of the bath seen for an ETH Hamiltonian is not present in the case of a MBL Hamiltonian, see Fig S7.

II. ELECTRON PARAMAGNETIC RESONANCE SPECTRUM

The aim of this section is to show how we compute numerically the EPR spectra. For this we need to extend the results of [68] to the nonsecular case in which the stationary density matrix ρ_{stat} possesses non-zero coherences in the eigenbasis of the system Hamiltonian. This provides the formula (S63) for a smoothed EPR spectrum which is appropriate for numerical evaluation.

We recall that after the $\pi/2$ pulse (performed in the stationary state at a time that we note $\tau = 0$) the density matrix gets transformed into $\rho_{\pi/2} = e^{i\frac{\pi}{2}S_i^x} \rho_{\text{stat}} e^{-i\frac{\pi}{2}S_i^x}$. The polarization of spin i is given at later times by

$$P_i^\mu(\tau) = 2\text{Tr}(S_i^\mu(\tau)\rho_{\pi/2}), \quad S_i^\mu(\tau) = e^{iH_S\tau} S_i^\mu e^{-iH_S\tau} \quad (\text{S55})$$

and we recall the quantity defined in the main text:

$$g_i(\tau) = (P_i^y - iP_i^x)(\tau) = -2i\text{Tr} \left[S_i^+(\tau)\rho_{\pi/2} \right] \quad (\text{S56})$$

Note that in our formalism the steady-state density matrix ρ that we get numerically is expressed in the (x, y) plane in the rotating frame at frequency ω_{MW} , whereas ρ_{stat} is in the fixed frame. Their relationship is $\rho_{\text{stat}} = U_{\text{MW}}(\tau)\rho U_{\text{MW}}(\tau)^\dagger$.

The polarization on the z axis (which is an invariant axis) in the steady-state can be computed with either density matrix. Indeed,

$$\text{Tr}(S_i^z \rho_{\text{stat}}) = \sum_{n,m} e^{i\omega_{\text{MW}}(s_m^z - s_n^z)\tau} \rho_{nm} \langle m | S_i^z | n \rangle = \sum_{\substack{n,m \\ s_n^z = s_m^z}} \rho_{nm} \langle m | S_i^z | n \rangle = \text{Tr}(S_i^z \rho) \quad (\text{S57})$$

as $\langle m | S_i^z | n \rangle$ vanishes outside the blocks of constant S^z (defined by $s_m^z = s_n^z$).

In the following we focus on the EPR spectrum instead. First, to express the post-pulse polarization with ρ instead of $\rho_{\pi/2}$, we write

$$e^{i\frac{\pi}{2}S_i^x} = \cos \frac{\pi}{4} + 2iS_i^x \sin \frac{\pi}{4} = \frac{1}{\sqrt{2}} (\mathbb{1} + 2iS_i^x) \quad (\text{S58})$$

Starting from the definition Eq. (S56) :

$$g_i(\tau) = -i \sum_{k,l,m,n} e^{i\tau[\varepsilon_k - \varepsilon_l + \omega_{\text{MW}}(s_m^z - s_n^z)]} \langle m| 1 - 2iS_i^x |k\rangle \langle k| S_i^+ |l\rangle \langle l| 1 + 2iS_i^x |n\rangle \rho_{nm} \quad (\text{S59})$$

We thus expect the frequency spectrum to be a sum of exponentially many Dirac delta peaks. In order to smooth the spectrum we shall average over a small frequency window $\delta\omega$, *i.e.* we compute the EPR spectrum as

$$\tilde{f}(\omega) = \frac{1}{N} \sum_{i=1}^N \frac{1}{\delta\omega} \int_{\omega}^{\omega + \delta\omega} f_i(\omega) \, d\omega, \quad f_i(\omega) = \text{Re} \left[\int_0^\infty \frac{d\tau}{\pi} g_i(\tau) e^{-i\omega\tau - \eta\tau} \right] \quad (\text{S60})$$

where we introduce a small cutoff $\eta > 0$. In essence we have to regularize integrals using a Cauchy principal value over finite intervals of length $\delta\omega$. We indeed note that

$$\int_0^\infty \frac{d\tau}{\pi} e^{-i(\omega - \omega_0)\tau - \eta\tau} = \frac{1}{\pi} \frac{1}{i(\omega - \omega_0) + \eta} = \frac{\eta/\pi}{(\omega - \omega_0)^2 + \eta^2} - \frac{i}{\pi} \frac{\omega - \omega_0}{(\omega - \omega_0)^2 + \eta^2} \quad (\text{S61})$$

The real part is a Lorentzian and will act as $\delta(\omega - \omega_0)$ for $\eta \rightarrow 0^+$ while the other (principal value) imaginary part remains integrable around $\omega = \omega_0 \forall \eta > 0$ (with a slope $\propto \eta^{-2}$).

Performing the Fourier transforms yields

$$\begin{aligned} \tilde{f}(\omega) = & \frac{1}{N\delta\omega} \sum_{k,l,m,n} \text{Re} \left\{ \left[\mathbb{1}(\omega_{klmn} \in I_\omega) - \frac{i}{\pi} \ln \left| \frac{\omega + \delta\omega - \omega_{klmn}}{\omega - \omega_{klmn}} \right| \right] \right. \\ & \left. \times \rho_{nm} \sum_i \langle m| 1 - 2iS_i^x |k\rangle \langle k| S_i^+ |l\rangle \langle l| 1 + 2iS_i^x |n\rangle \right\} \end{aligned} \quad (\text{S62})$$

where $I_\omega = [\omega, \omega + \delta\omega]$ and $\omega_{klmn} = \varepsilon_k - \varepsilon_l + \omega_{\text{MW}}(s_m^z - s_n^z)$. The index function $\mathbb{1}$ is 1 if true and 0 else. The interval of EPR frequencies experimentally probed is centered around ω_e . So, as the energy scales between different polarization sectors are well separated, the terms between brackets in the first line are negligible unless $s_k^z - s_l^z + s_m^z - s_n^z = 1$. Yet the factor $\langle k| S_i^+ |l\rangle$ implies $s_k^z - s_l^z = 1$, thus considering only matrix elements such that $s_m^z = s_n^z$ is enough to compute the EPR spectrum.

This means in the second line of Eq. (S62) the polarization from $|n\rangle$ to $|m\rangle$ must not change. As S_i^+ performs polarization jumps of +1, we can get rid of the non-polarization-conserving terms and get, relabeling indices,

$$\begin{aligned} \tilde{f}(\omega) = & \frac{1}{N\delta\omega} \sum_{n,k} \text{Re} \left\{ \left[\mathbb{1}(\omega_{nk} \in I_\omega) - \frac{i}{\pi} \ln \left| \frac{\omega + \delta\omega - \omega_{nk}}{\omega - \omega_{nk}} \right| \right] \right. \\ & \left. \times \left[\sum_{\substack{m \\ s_m^z = s_n^z}} \rho_{mn} \sum_i \langle n| S_i^+ |k\rangle \langle k| S_i^- |m\rangle - \sum_{\substack{m \\ s_m^z = s_k^z}} \rho_{km} \sum_i \langle m| S_i^- |n\rangle \langle n| S_i^+ |k\rangle \right] \right\} \end{aligned} \quad (\text{S63})$$

Note that if the density matrix is diagonal in the eigenbasis, this implies

$$\tilde{f}(\omega) = \frac{1}{N\delta\omega} \sum_{n,k} \mathbb{1}(\omega_{nk} \in I_\omega) (\rho_{nn} - \rho_{kk}) \sum_i \left| \langle n| S_i^+ |k\rangle \right|^2 \quad (\text{S64})$$

which agrees with the result of [68, Eq.(23)]. In this case we have, noting $f(\omega) = \sum_i f_i(\omega)/N$ (for $\eta \rightarrow 0^+$):

$$f(\omega) = \frac{1}{N} \sum_i \sum_{n,m} \delta(\omega - \omega_{nm}) (\rho_{nn} - \rho_{mm}) \left| \langle n| S_i^+ |m\rangle \right|^2 \quad (\text{S65})$$

and only the gaps $\omega_{nm} \approx \omega_e$ with $s_n^z = s_m^z + 1$ actually contribute to the sum. So writing this set as an approximate interval (for large N) $I = \{\omega_{nm} \text{ with } s_n^z = s_m^z + 1\}$ where the EPR spectrum is non zero, one gets, using $[S_i^+, S_i^-] = 2S_i^z$,

$$\int_I d\omega f(\omega) = \frac{1}{N} \sum_i \left[\sum_n \rho_{nn} \langle n| S_i^+ S_i^- |n\rangle - \sum_m \rho_{mm} \langle m| S_i^- S_i^+ |m\rangle \right] = \frac{2}{N} \sum_i \text{Tr}(S_i^z \rho) = \frac{2 \langle S^z \rangle}{N} = P^z \quad (\text{S66})$$

i.e. the integral of the EPR spectrum gives the total polarization along z , P^z .

Finally, for the more trivial case of non-interacting spins⁸ with Hamiltonian $H_S = \sum_i (\omega_e + \Delta_i) S_i^z = \sum_i \omega_i S_i^z$, the previous integral holds as it is a particular case, but more precisely in Eq. (S65) at fixed spin i the transition

⁸ Note however that there the gaps are largely degenerated and one must take this into account in our dynamical equations.

$\langle n | S_i^+ | m \rangle$ is non-zero iff $\omega_{nm} = \omega_i$, so that we can factor out the Dirac delta function and get

$$f(\omega) = \frac{1}{N} \sum_i \delta(\omega - \omega_i) \sum_{n,m} (\rho_{nn} - \rho_{mm}) \left| \langle n | S_i^+ | m \rangle \right|^2 = \frac{1}{N} \sum_i P_i^z \delta(\omega - \omega_i) \quad (\text{S67})$$

where $P_i^z = 2\text{Tr}(S_i^z \rho)$. This last equation exhibits a connection between EPR and polarization profiles for non-interacting spins.

III. BATH-INDUCED LOCALIZATION BY TEMPERATURE VARIATION: ADDITIONAL NUMERICAL RESULTS

A. Thermal mixing and spin temperature behavior

It has been shown in Refs. [41–43] within the secular GKLS equation and the Hilbert approximation that there exists a remarkable situation of *thermal mixing* where the driven system behaves as an effective equilibrium steady state. It can be thought as an effective Gibbs ensemble with two parameters conjugated to the two conserved quantities of the isolated (microcanonical) system with Hamiltonian H_S , which are the energy and the total spin along z . We note ρ^{stat} the steady-state distribution, which is then diagonal in the eigenstate basis:

$$\rho_{nn}^{\text{stat}} \propto e^{-\beta_S(\varepsilon_n - h s_n^z)} \quad (\text{S68})$$

where β_S is the so-called *spin temperature* conjugated to the energy and h is the effective magnetic field conjugated to the spin along z .

In the Hilbert approximation Eq. (S52), the transition rates define several timescales. In the following for simplicity we assume that the two S_i^z transitions timescales are equal, and we note their common value $T_z = T(0) = T^*$. We shall comment later what happens when they differ. $T_1 = 2T(\omega_e)$ is the relaxation time of the system⁹, and therefore can be considered as the longest timescale. If we assume $T_z \ll T_1$ then the main timescales are:

- T_1 the bath relaxation timescale induced by S_i^x or S_i^y flipping of the spins with associated energy $\omega \approx \pm \omega_e$. At $T = 1.2$ K these flips strongly favor the approximate ground state of all spins down: $h(\omega \simeq \omega_e) \simeq 0.98$ and $h(\omega \simeq -\omega_e) \approx 0.02$.
- T_z the bath relaxation timescale due to S_i^z flips with energy $|\omega_{nm}| \ll \omega_e$. Such flips do not particularly favor any sign of the spin i , as $h(\omega_{nm}) \simeq 1/2$ is quasi independent of the transition ω_{nm} .
- The microwave time

$$\frac{1}{W_{nm}^{\text{MW}}} = \frac{1 + (T_{nm} \Delta \omega_{nm})^2}{2\omega_1^2 T_{nm} \left| \langle n | S^x | m \rangle \right|^2} \quad (\text{S69})$$

defined in Eq. (S53). These timescales depend on n and m but the shortest ones (*i.e.* most efficient transitions) are such that $|\langle n | S^x | m \rangle|$ is not too low and $\Delta \omega_{nm} \simeq 0$ is near resonance. Therefore, as $T_{nm} \sim T_z$, this time may be assessed through a simple Lorentzian rate

$$\frac{1}{T^{\text{MW}}(\Delta \omega)} = \frac{\omega_1^2 T_z}{1 + (\Delta \omega T_z)^2} \quad (\text{S70})$$

of width $\Delta \omega \sim 1/T_z$ and minimal typical value $T_{\min}^{\text{MW}} = (\omega_1^2 T_z)^{-1}$.

- The Thouless time T_D is the typical dephasing timescale $1/\Delta \omega_{nm}$ in the coherence dynamics Eq. (S48), which is roughly given by the interaction and disorder timescales $T_D = \min(1/U, 1/\Delta \omega_e)$.

This phase is characterized by an inhomogeneity of the polarization profile between the spins when the spin temperature is low. In a nutshell this occurs when the microwaves are effective in a short frequency range, which thus resonate with a small number of transitions ω_{nm} . Consequently they affect a small number of spins. But as shown in Refs. [41–43], thermal mixing happens when the interactions strong enough, typically where the system

⁹ The factor 2 is conventionally defined to recover the Bloch solution [52] by solving exactly the single-spin case $N = 1$ with $H_S = \omega_e S_1^z$,

$$\text{Tr} \left(S_1^z \rho^{\text{stat}} \right) = \frac{M_0}{1 + \frac{T_1}{T_{\text{MW}}}} ,$$

$$\begin{aligned} T_{\text{MW}} &= \frac{1 + (\omega_e - \omega_{\text{MW}})^2 T_2^2}{T_2 \omega_1^2} , \\ \frac{1}{T_2} &= \frac{1}{4T(0)} + \frac{1}{4T(\omega_e)} , \\ M_0 &= -\frac{1}{2} \tanh \left(\frac{\beta \omega_e}{2} \right) = \frac{\text{Tr} \left(S_1^z e^{-\beta \omega_e S_1^z} \right)}{\text{Tr} e^{-\beta \omega_e S_1^z}} . \end{aligned}$$

Hamiltonian satisfies ETH. The spins then share the polarization and arrange into a characteristic polarization profile, characterized by an approximately linear relation $P(\omega_i)$ with $\omega_i = \omega_e + \Delta_i$ the typical frequency of spin i .

A difficulty in observing the spin-temperature behavior is that the same timescale T_z controls several competing physical processes. It is the main timescale in the nonsecular terms for $T_z \ll T_1$. In the secular terms (S48), it (i) enters in the microwave timescales as is clearly visible in the Hilbert approximation (S52) (ii) it enters the evolution of the diagonal elements, inducing the homogenization of the polarization profile as these S^z transitions flip equally spins + or - (for this reason it is called *spectral diffusion*) (iii) participates out of the diagonal in the decoherence process through T_{nm} .

Within the nonsecular GKSL equation (S46), we are able to recover a marked spin-temperature behavior under the following necessary conditions:

1.

$$\boxed{\Delta\omega_e \lesssim U} \quad (S71)$$

meaning that the spin-temperature phase needs enough interactions for ETH to hold. Note that especially if N is small the inequality is not sharp.

2.

$$\boxed{T_z \gg T_D \text{ (Thouless time)} \simeq \min\left(\frac{1}{U}, \frac{1}{\Delta\omega_e}\right)} \quad (S72)$$

In the coherence dynamics, the dephasing dominate the nonsecular terms and the Hilbert approximation is valid.

3.

$$\boxed{T_1 T_z \omega_1^2 \gtrsim 1 \quad \Leftrightarrow \quad T_{\min}^{\text{MW}} \lesssim T_1} \quad (S73)$$

The microwaves are effective at least for the resonant gaps (otherwise the system would thermalize with Boltzmann distribution).

4.

$$\boxed{\omega_1 \sqrt{\frac{T_1}{T_z}} \lesssim \max(U, \Delta\omega_e)} \quad (S74)$$

$\omega_1 \sqrt{T_1/T_z}$ is the maximal frequency range for which $T^{\text{MW}}(\Delta\omega) < T_1$ under the previous condition Eq. (S73), *i.e.* the frequency window over which the microwaves are effective. This range needs to be narrower than the typical frequency range $\max(U, \Delta\omega_e)$ which is probed in the EPR experiment (*i.e.* frequencies around ω_e which correspond to gaps of S_i^+). Otherwise, most transitions are irradiated and all spins feel the microwaves, which has a tendency to thermalize them at infinite temperature (*i.e.* $\text{Tr}(S_i^z \rho_{\text{stat}}) = 0$). This is needed to create some inhomogeneity within the spins.

5.

$$\boxed{T_z \lesssim T_1} \quad (S75)$$

This emphasizes that if T_1 is too large then spectral diffusion will dominate and the profile will be homogeneous (high spin temperature). A way to keep spectral diffusion low is to make the two timescale differ such that

$$\boxed{T(0) \ll T^*} \quad (S76)$$

Indeed $T(0)$ enters only in T_{nm} (S19), *i.e.* in the decoherence process off the diagonal of Eq. (S48), while T^* appears in the bath transitions (S19) on the diagonal which determine directly the steady-state values.

6.

$$\boxed{\omega_1 T_z \gtrsim 1 \quad \Leftrightarrow \quad T_{\min}^{\text{MW}} \lesssim T_z} \quad (S77)$$

This is again to prevent spectral diffusion to destroy the spin-temperature behavior.

The spin-temperature shapes of the EPR spectrum are displayed in Fig. 3 of the main text. In Fig. S6 we show the corresponding polarization profiles in the ETH phase.

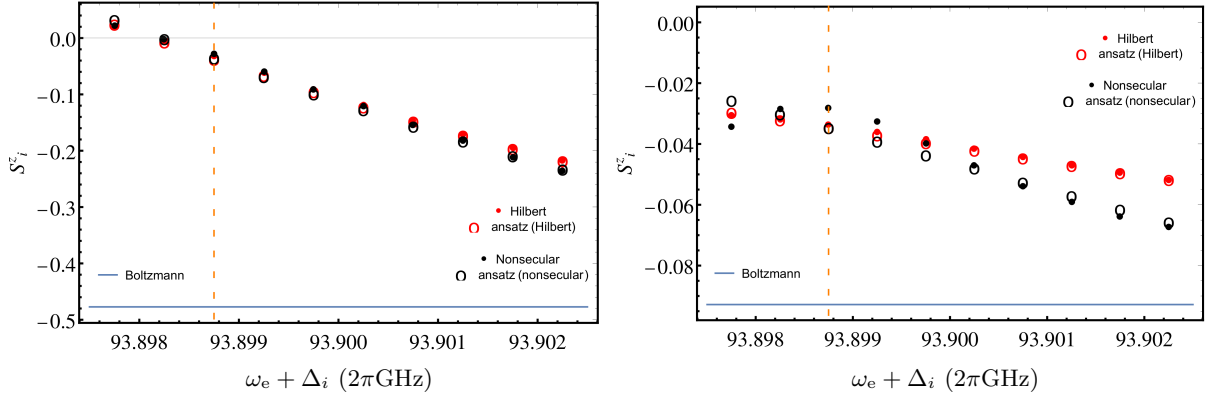


FIG. S6. Polarization profiles (red : Hilbert, black : nonsecular) for $N = 10$ spins with $\Delta\omega_e = 5 \cdot 2\pi\text{MHz}$ and $U = 0.75 \cdot 2\pi\text{MHz}$ (ETH eigenstates). The bath and microwave parameters are given in Table 1 of the main text ($T_1 = 10^4(2\pi\text{GHz})^{-1}$, $T^* = T(0) = 10^3(2\pi\text{GHz})^{-1}$). The vertical dashed line points out the microwave frequency. The horizontal blue line is the Boltzmann prediction. Full dots are the numerical results ; hollow circles are obtained by the spin-temperature ansatz (S78). (left) $\beta^{-1} = 1.2$ K. The bath is slow and as a consequence nonsecular and Hilbert dynamics yield similar spin-temperature curves. (right) $\beta^{-1} = 12$ K. Here the bath timescales are short and the full (nonsecular) dynamics gets localized : only the near-resonant spins feel the microwaves, as if they were non interacting, causing the hole burning. Each profile has been averaged over 1000 realizations of disorder and interactions for the nonsecular case and 3000 realizations for the Hilbert case.

B. Estimating the spin-temperature ansatz parameters from simulation data

Here we give details about the numerical computation of the spin-temperature ansatz parameters. The spin-temperature ansatz is

$$\rho_{nn}^{\text{ans}}(\beta_s, h) \propto e^{-\beta_s(\varepsilon_n - hs_n^z)} \quad (\text{S78})$$

We solve numerically for (β_s, h) to match the average energy and polarization in the stationary state [42]

$$\begin{cases} \text{Tr}(H_S \rho^{\text{stat}}) = \sum_{n=1}^{2^N} \varepsilon_n \rho_{nn}^{\text{ans}}(\beta_s, h) \\ \text{Tr}(S^z \rho^{\text{stat}}) = \sum_{n=1}^{2^N} s_n^z \rho_{nn}^{\text{ans}}(\beta_s, h) \end{cases} \quad (\text{S79})$$

through an iterative procedure, starting from the initial guess

$$\begin{cases} \beta_s = \frac{2N}{\Delta\omega_e} \text{argth } P_n^{\text{stat}} \\ h = \omega_{\text{MW}} \end{cases} \quad (\text{S80})$$

where the nucleus polarization is [69]

$$P_n^{\text{stat}} = \frac{\int d\omega d(\omega) d(\omega + \omega_n) [P_{\text{stat}}^z(\omega) - P_{\text{stat}}^z(\omega + \omega_n)]}{\int d\omega d(\omega) d(\omega + \omega_n) [1 - P_{\text{stat}}^z(\omega) P_{\text{stat}}^z(\omega + \omega_n)]} \simeq \frac{2 \sum_{i=1}^{N-1} [\text{Tr}(S_i^z \rho^{\text{stat}}) - \text{Tr}(S_{i+1}^z \rho^{\text{stat}})]}{\sum_{i=1}^{N-1} [1 - 4 \text{Tr}(S_i^z \rho^{\text{stat}}) \text{Tr}(S_{i+1}^z \rho^{\text{stat}})]} \quad (\text{S81})$$

ω_n is the nucleus Zeeman gap. $d(\omega)$ is the disorder distribution at energy ω ; the second equality comes from considering the disorder as uniform and the typical frequency between two spins $\omega_i - \omega_{i+1} \approx \omega_n$, where $\omega_i = \omega_e + \Delta_i$ is the frequency of spin i in a non-interacting picture. We finally check that for all spins $\text{Tr}(S_i^z \rho^{\text{ans}}) = \text{Tr}(S_i^z \rho^{\text{stat}})$ in order to control that the ansatz reproduces well the data.

Here the polarization of a coupled nucleus enters explicitly. Note that in this work we focused on the electronic spins only, as their out-of-equilibrium steady state is the crucial feature concerning DNP in the thermal mixing regime. The electronic polarization is indeed transferred to the nuclei, the polarization of interest in DNP *in fine*. One can actually add a nucleus to the spin system to check the polarization transfer; this has been studied in Ref. [42].

C. Hole burning

A very different situation where spins do not have collective behavior is for example when the disorder is strong [41–43], in the phase where the eigenstates are many-body localized. Then only spins resonant with the

microwave feel them and acquire a vanishing polarization, while the others are unaffected by the driving, as if they were independent spins. The polarization profile results in a hole burning shape. We showed in this article that if the coupling to the bath is strong enough, the nonsecular terms may induce this hole burning shape as well in the ETH phase, as if spins resonant with the microwaves were again localized with respect to the others.

The necessary conditions for this bath-induced localization to take place are 1, 3 and 4 of Sec. III A but now the nonsecular terms need to be as important as possible to dominate over dephasing. This means we take $T^* = T(0) = T_z$ with

$$T_z \lesssim T_D \text{ (Thouless time)} \simeq \min \left(\frac{1}{U}, \frac{1}{\Delta\omega_e} \right) \quad (\text{S82})$$

Note that the rate of the $1/T_{nm}$ decoherence term is as well controlled by T_z .

The hole burning at high temperature is visible in the ETH phase in Fig. S6(right) for the polarization and in Fig. 3(bottom) of the main text for the EPR spectrum. In Fig. S7 we show that if the Hamiltonian eigenstates are MBL, one gets, independently of the chosen dynamics and temperatures, a hole burning behavior.

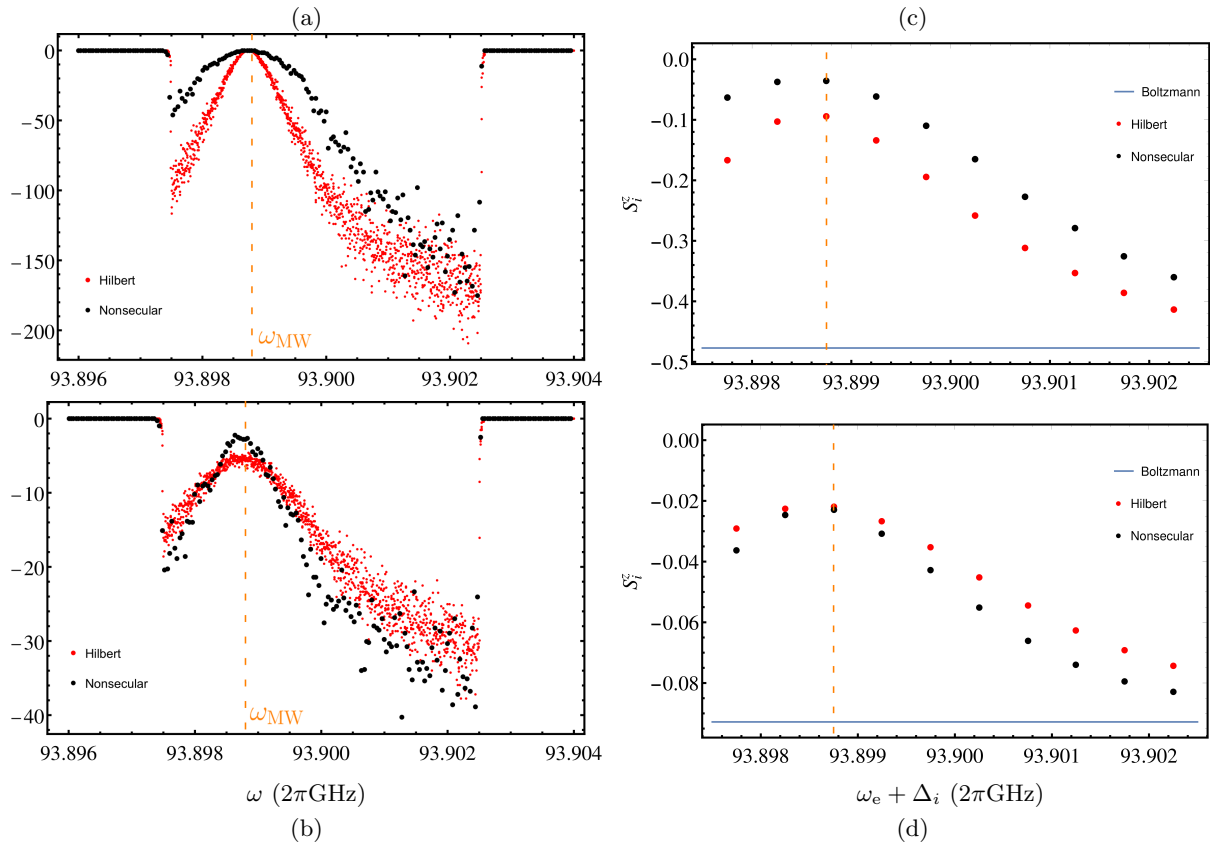


FIG. S7. Numerical profiles (red : Hilbert, black : nonsecular) for $N = 10$ spins with $\Delta\omega_e = 5 \cdot 2\pi\text{MHz}$ and $U = 0.1 \cdot 2\pi\text{MHz}$ (MBL eigenstates). The bath and microwave parameters for each temperature are given in the main text. The vertical dashed line points out the microwave frequency. Average is taken over 1000 realizations of disorder and interactions for the nonsecular case and 10000 realizations in the Hilbert case. $\beta^{-1} = 1.2$ K in the top figures ; $\beta^{-1} = 12$ K in the bottom figures. (a)(b) EPR spectra. Frequency bins are ten times larger in the nonsecular case than in the Hilbert case. (c)(d) Polarization profiles. The horizontal blue line is the Boltzmann prediction.

Here we note a hole burning shape for both temperatures. There is no qualitative effect of nonsecularity : nonsecular terms are small for MBL eigenstates as mentioned in Sec. IF.

In the data exhibited in the main text we have chosen T_1 to be the longest timescale (the other timescale of the nonsecular terms being T^*). In Fig. S8 we display the EPR and polarization profiles obtained for the same system as in Fig. 3(bottom) of the main text (see Fig. S6) but with $T_1 \ll T^*$. We obtain again a breakdown of thermal mixing.

In Fig. S9 we show that one can get an even more impressive localization effect from the nonsecular GKSL equation without disorder. This is achieved for $N = 12$ spins by pushing the bath relaxation times to less realistic values and irradiating only a single spin (namely, the third one). In the Hilbert approximation, the 12 spins share the same polarization owing to the strong interaction. All spins feel the microwaves. But in the nonsecular dynamics, despite the strong interaction, the third spin is put to infinite temperature ($\text{Tr}(S_3^z \rho_{\text{stat}}) = 0$) whereas all other spins are at Boltzmann equilibrium.

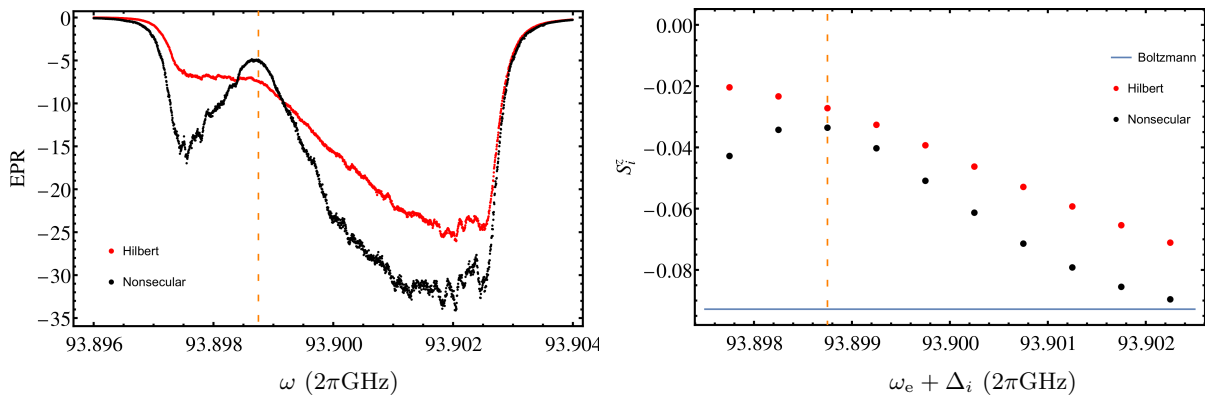


FIG. S8. Polarization profiles (red : Hilbert, black : nonsecular) for $N = 10$ spins with $\Delta\omega_e = 5 \cdot 2\pi\text{MHz}$ and $U = 0.75 \cdot 2\pi\text{MHz}$ (ETH eigenstates) $\beta^{-1} = 12$ K. The bath and microwave parameters are $T_1 = 10^4(2\pi\text{GHz})^{-1} = 1.6\ \mu\text{s}$, $T^* = 5 \cdot 10^5(2\pi\text{GHz})^{-1} = 80\ \mu\text{s}$, $T(0) = 2 \cdot 10^4(2\pi\text{GHz})^{-1} = 3.2\ \mu\text{s}$. (left) EPR spectrum. (right) Polarization profiles. The vertical dashed line points out the microwave frequency. The horizontal blue line is the Boltzmann prediction. Each profile has been averaged over 1000 realizations of disorder and interactions for the nonsecular case and 3000 realizations for the Hilbert case.

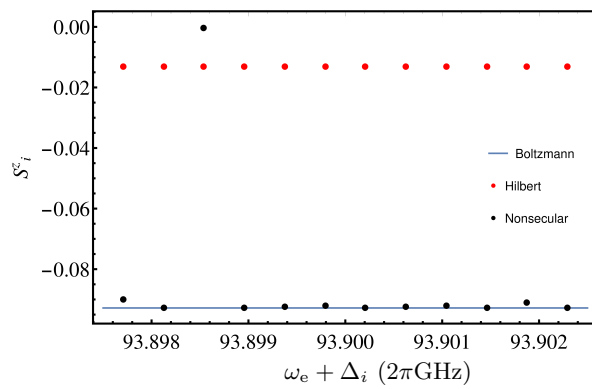


FIG. S9. Polarization profile for a setup exhibiting a very strong localization, for $N = 12$ spins at $\beta^{-1} = 12$ K (red : Hilbert, black : nonsecular). The data corresponds to a single typical sample where disorder is negligible ($\Delta\omega_e = 10^{-4} \cdot 2\pi\text{MHz}$, essentially to ensure that the gaps are non degenerate) and the interaction is $U = 2\pi\text{ MHz}$. The microwaves irradiate *only* the third spin, with frequency $\omega_{\text{MW}} = \omega_e$ and strong amplitude $\omega_1 = 0.1 \cdot 2\pi\text{GHz}$. The nonsecular terms are very effective due to the very low value of $T(0) = T^* = 0.1 \cdot (2\pi\text{GHz})^{-1} = 10^{-10}/2\pi\text{ s}$; $T_1 = 10^{-4}/2\pi\text{ s}$.

D. Spectral properties of the stationary state

In this section we provide additional data concerning the spectral properties of the steady-state density matrix ρ_{stat} in the Hilbert or nonsecular cases. We emphasize that, for all the $N = 10$ data, the sample-to-sample fluctuations are quite well concentrated on the averages displayed.

In Fig. S10 we provide the eigenvalue distribution of the stationary density matrix, for parameters where the nonsecular dynamics leads to a hole burning while the Hilbert one yields a spin-temperature shape. This is to show that the distribution is not dominated by a small number of eigenstates ; all of them are relevant. Moreover, the distribution in both dynamics are similar : the qualitative difference in steady-state observables does not come from this population distribution but finds an explanation in the eigenstates' statistics, as explained in the main text.

It is pointed out in the main text that the when when the bath induces localization in the system, the eigenstates reached by the density matrix in the long-time limit are different from the Hamiltonian ones. They do not satisfy ETH : are less entangled and more akin to MBL eigenstates. Now we focus on the more extreme case introduced at the end of Sec. III C: 12 homogeneous spins, only spin 3 irradiated with strong nonsecular effects. Here the localization is “complete” : spin 3 decouples from the rest of the system, in spite of the strong interactions. In Fig. S11 we demonstrate that the eigenstates of the density matrix is not anymore the ETH Hamiltonian eigenstates but are pure states factorized on each individual spin basis, *i.e.* all S_i^z are good quantum numbers to describe this eigenbasis ; it corresponds to the Hamiltonian basis for non-interacting spins $U = 0$. Here the measurements performed by the bath modes wipe out all interaction in the many-body system. The entanglement entropy of each eigenstate is thus zero. The eigenvalue distribution of the matrix is much closer to the Boltzmann one than the Hilbert one.

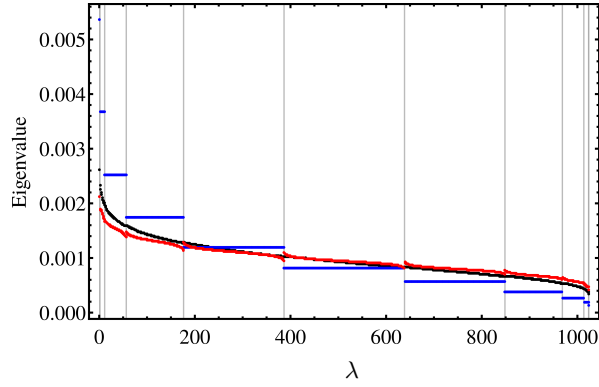


FIG. S10. Eigenvalues (populations) $\langle \lambda | \rho_{\text{stat}} | \lambda \rangle$ of the stationary density matrix ($|\lambda\rangle$ are eigenvectors), classified on the horizontal axis by increasing energy $\langle \lambda | H_S | \lambda \rangle$. Parameters correspond to those of Fig. S6 for $N = 10$ spins. Vertical gray lines delimit sectors of constant polarization (for Hamiltonian eigenstates). Blue : Boltzmann equilibrium $\rho_{\text{stat}} \propto \exp(-\beta H_S)$. Red : Hilbert solution. For the latter cases, the eigenvectors $|\lambda\rangle = |n\rangle$ are those of the Hamiltonian. Black : nonsecular solution.

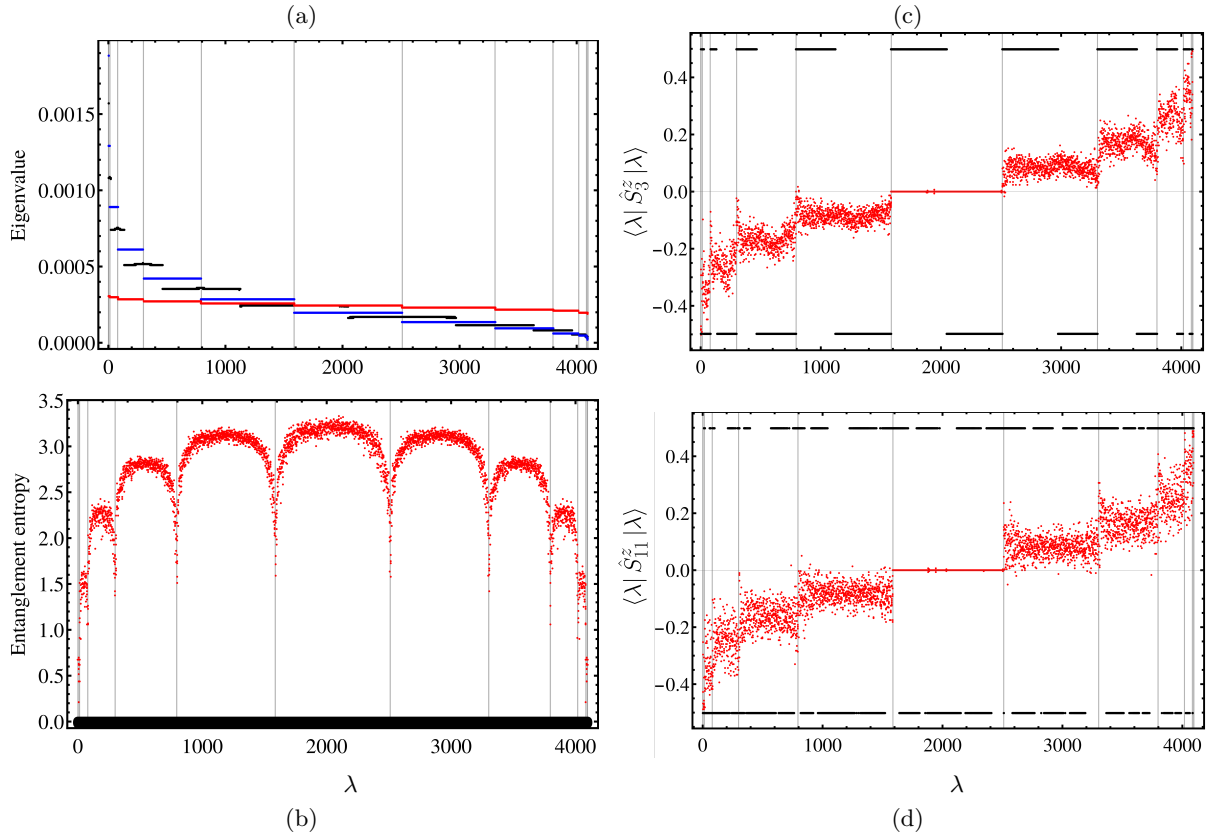


FIG. S11. The setting corresponds to the fully localized one with 12 spins introduced at the end of Sec. III C. Index λ is classified on the horizontal axis by increasing energy $\langle \lambda | H_S | \lambda \rangle$ ($|\lambda\rangle$ are eigenvectors of ρ_{stat}). Blue : Boltzmann equilibrium $\rho_{\text{stat}} \propto \exp(-\beta H_S)$. Red : Hilbert solution. For the latter cases, the eigenvectors $|\lambda\rangle = |n\rangle$ are those of the Hamiltonian. Black : nonsecular solution. Vertical gray lines delimit sectors of constant polarization (for Hamiltonian eigenstates). (a) Eigenvalues (populations) $\langle \lambda | \rho_{\text{stat}} | \lambda \rangle$ of ρ_{stat} . (b) Entanglement entropy of each eigenvector. Partial trace is taken over spins 6 to 12. (c) Expectation value of the observable S_3^z . (d) Same for S_{11}^z , qualitatively close to any other spin.

IV. A TOY MODEL FOR ZENO LOCALISATION

In this section, we analyze a toy model introduced in Fig. 2 of the main text. It presents similar features to the many-body DNP model with the advantage of possessing an analytical solution. We put hats on some operators to avoid possible confusion with scalar quantities.

Let us consider a three-level system (states labeled 0, 1, 2) subject to a monochromatic microwave perturbation that only couples the ground state $|0\rangle$ and the state $|1\rangle$. The system is coupled to two uncorrelated harmonic baths that allow exchange of energy between the ground state and the excited states. The Hamiltonian reads

$$H = H_S + H_{\text{MW}}(t) + H_{\text{int}} + H_B =$$

$$= \begin{pmatrix} 0 & V^* e^{i\omega_{\text{MW}} t} + \hat{B}_1^\dagger & \hat{B}_2^\dagger \\ V e^{-i\omega_{\text{MW}} t} + \hat{B}_1 & \omega_e - \Delta & J \\ \hat{B}_2 & J & \omega_e + \Delta \end{pmatrix} + \sum_{\alpha=1,2} \sum_k \Omega_k \hat{a}_{\alpha k}^\dagger \hat{a}_{\alpha k} \quad (\text{S83})$$

$$\hat{B}_\alpha = \sum_k g_{\alpha k} \hat{a}_{\alpha k} \quad (\text{S84})$$

The Born-Markov master equation (S7) (no secular approximation is involved) for the system density matrix ρ in the Schrödinger representation has the form

$$\frac{d\rho}{dt} = -i [H_S + H_{\text{MW}}, \rho] - \int_0^\infty d\tau \text{Tr}_B \left\{ \left[H_{\text{int}}, \left[e^{-i(H_S+H_B)\tau} H_{\text{int}} e^{i(H_S+H_B)\tau}, \rho \otimes \rho_B \right] \right] \right\}. \quad (\text{S85})$$

It does not depend on the choice of basis in the system subspace and thus does not privilege the eigenbasis of H_S . Assuming $J, \Delta \ll \omega_e$, we approximate

$$e^{-i(H_S+H_B)\tau} H_{\text{int}} e^{i(H_S+H_B)\tau} \approx \sum_{\alpha=1,2} |\alpha\rangle\langle 0| \sum_k g_{\alpha k} \hat{a}_{\alpha k} e^{i(\Omega_k - \omega_e)\tau} + \text{H.c.} \equiv \sum_{\alpha=1,2} |\alpha\rangle\langle 0| \hat{B}_\alpha(-\tau) e^{-i\omega_e\tau} + \text{H.c.} \quad (\text{S86})$$

with $\hat{B}_\alpha(\tau) = \sum_k g_{\alpha k} e^{-i\Omega_k \tau} \hat{a}_{\alpha k}$ the dynamical evolution of the bath modes. When performing the trace over the bath modes, assuming the bath has no fine structure on the scale J, Δ , we must only evaluate the following bath correlators at frequency ω_e (and their complex conjugates):

$$\int_0^\infty d\tau e^{i\omega_e\tau} \left\langle \hat{B}_\alpha^\dagger(0) \hat{B}_\beta(\tau) \right\rangle_B = \delta_{\alpha\beta} \sum_k \frac{i|g_{\alpha k}|^2 n_{\alpha k}}{\omega_e - \Omega_k + i0^+} \equiv \delta_{\alpha\beta} [\gamma_\alpha \bar{n}_\alpha + i\delta_\alpha], \quad (\text{S87})$$

$$\int_0^\infty d\tau e^{i\omega_e\tau} \left\langle \hat{B}_\alpha(\tau) \hat{B}_\beta^\dagger(0) \right\rangle_B = \delta_{\alpha\beta} \sum_k \frac{i|g_{\alpha k}|^2 (n_{\alpha k} + 1)}{\omega_e - \Omega_k + i0^+} \equiv \delta_{\alpha\beta} [\gamma_\alpha (\bar{n}_\alpha + 1) + i\delta'_\alpha], \quad (\text{S88})$$

$n_{\alpha k} = (e^{\beta\Omega_k} - 1)^{-1}$ and $\bar{n}_\alpha = (e^{\beta\omega_e} - 1)^{-1}$ are Bose-Einstein distributions, $\gamma_\alpha \propto |g_{\alpha k}|^2|_{k \leftrightarrow \omega_e}$ and the Lamb-shifts $\delta_\alpha, \delta'_\alpha$ can be expressed through Cauchy principal values. The resulting master equation has the GKSL form

$$\dot{\rho} = -i [H_S + H_{\text{LS}} + H_{\text{MW}}, \rho] + \mathcal{D}_1(\rho) + \mathcal{D}_2(\rho)$$

$$H_{\text{LS}} \equiv \sum_{\alpha=1,2} \delta'_\alpha |\alpha\rangle\langle\alpha| - \delta_\alpha |0\rangle\langle 0| \quad \mathcal{D}_\alpha(\rho) \equiv L_\alpha \rho L_\alpha^\dagger + \tilde{L}_\alpha \rho \tilde{L}_\alpha^\dagger - \frac{1}{2} \left\{ L_\alpha^\dagger L_\alpha + \tilde{L}_\alpha^\dagger \tilde{L}_\alpha, \rho \right\}$$

$$L_\alpha = \sqrt{2\gamma_\alpha \bar{n}_\alpha} |\alpha\rangle\langle 0| \quad \tilde{L}_\alpha = \sqrt{2\gamma_\alpha (\bar{n}_\alpha + 1)} |0\rangle\langle\alpha| \quad (\text{S89})$$

Let us make here a few comments on this GKSL equation to make contact with our DNP model:

1. This equation is identical to the one obtained through Ref. [58]'s approach employed in the DNP model. Indeed one can project the usual Born-Markov equation (S7) on eigenstates and get the same jump operators for $\Delta, J \ll \omega_e$. Alternatively, one can directly compute Ref. [58]'s nonsecular jump operators (defined in Eq.(6) of the main text) by redefining slightly the system in order to satisfy the hypothesis that H_{int} is written as a sum of Hermitian operators : $H_{\text{int}} = \sum_{\alpha=1,2} \hat{S}_\alpha \otimes \hat{B}_\alpha$ with $\hat{S}_\alpha = |\alpha\rangle\langle 0| + \text{H.c.}$, $\hat{B}_\alpha = \sum_k g_{\alpha k} \hat{b}_{\alpha k} + \text{H.c.}$, yielding the same result.
2. The toy model corresponds to a variant of our DNP model for $N = 2$ spins truncated to the three lowest levels, *i.e.* taking $|++\rangle = 0$ or density matrix elements $\langle \lambda | \rho | ++ \rangle$ for any vector $|\lambda\rangle$. More precisely, the relationship is $U_{12} \equiv J$ with fixed local disorder $\Delta_i \equiv \pm 2\Delta$ and energy levels shifted so that $H_S |--\rangle = 0$, only the spin 1 is irradiated at frequency ω_{MW} (with $V \equiv \omega_1/\sqrt{2}$) and the bath do not couple to S_i^z (*i.e.* $T^*, T(0) \rightarrow \infty$); for example one can consider $H_{\text{int}} = \sum_i S_i^x \otimes B_i^x$ which defines the parameters $\gamma_{1,2} \equiv \gamma(\omega_e)/8$. In this setting, the population of levels 1 and 2 in the 3-level model plotted in Fig. 2 of the main text gives directly the steady-state polarization of each spin: $\text{Tr}(S_i^z \rho) \equiv \rho_{ii} - \frac{1}{2}$.

In the following we neglect the Lamb-shifts δ . Explicitly in components,

$$\dot{\rho}_{11} = iV^*e^{i\omega_{\text{MW}}t}\rho_{01}^* - iVe^{-i\omega_{\text{MW}}t}\rho_{01} + iJ(\rho_{12} - \rho_{12}^*) + 2\gamma_1\bar{n}_1\rho_{00} - 2\gamma_1(\bar{n}_1 + 1)\rho_{11}, \quad (\text{S90})$$

$$\dot{\rho}_{22} = iJ(\rho_{12}^* - \rho_{12}) + 2\gamma_2\bar{n}_2\rho_{00} - 2\gamma_2(\bar{n}_2 + 1)\rho_{22}, \quad (\text{S91})$$

$$\dot{\rho}_{01} = i\omega_e\rho_{01} + iV^*e^{i\omega_{\text{MW}}t}(\rho_{00} - \rho_{11}) - i\Delta\rho_{01} + iJ\rho_{02} - [\gamma_1(2\bar{n}_1 + 1) + \gamma_2\bar{n}_2]\rho_{01}, \quad (\text{S92})$$

$$\dot{\rho}_{02} = i\omega_e\rho_{02} - iV^*e^{i\omega_{\text{MW}}t}\rho_{12} + iJ\rho_{01} + i\Delta\rho_{02} - [\gamma_2(2\bar{n}_2 + 1) + \gamma_1\bar{n}_1]\rho_{02}, \quad (\text{S93})$$

$$\dot{\rho}_{12} = 2i\Delta\rho_{12} - iVe^{-i\omega_{\text{MW}}t}\rho_{02} + iJ(\rho_{11} - \rho_{22}) - [\gamma_1(\bar{n}_1 + 1) + \gamma_2(\bar{n}_2 + 1)]\rho_{12}. \quad (\text{S94})$$

Looking for the solution with time-independent $\rho_{11}, \rho_{22}, \rho_{12}$ and $\rho_{01}, \rho_{02} \propto e^{i\omega_{\text{MW}}t}$ (we rename $\rho_{0\alpha} \rightarrow \rho_{0\alpha}e^{-i\omega_{\text{MW}}t}$), we arrive at a time-independent linear system. Let us for simplicity take $V = V^*$, $\gamma_1 = \gamma_2 \equiv \gamma$, and set $\bar{n}_\alpha = 0$ (*i.e.* zero temperature). Then the system has the form

$$0 = V(\rho_{01} - \rho_{01}^*) - J(\rho_{12} - \rho_{12}^*) - 2i\gamma\rho_{11}, \quad (\text{S95})$$

$$0 = J(\rho_{12} - \rho_{12}^*) - 2i\gamma\rho_{22}, \quad (\text{S96})$$

$$0 = (\omega_{\text{MW}} - \omega_e + \Delta - i\gamma)\rho_{01} - J\rho_{02} + V(2\rho_{11} + \rho_{22} - 1), \quad (\text{S97})$$

$$0 = -J\rho_{01} + (\omega_{\text{MW}} - \omega_e - \Delta - i\gamma)\rho_{02} + V\rho_{12}, \quad (\text{S98})$$

$$0 = V\rho_{02} - 2(\Delta + i\gamma)\rho_{12} + J(\rho_{22} - \rho_{11}). \quad (\text{S99})$$

Let us solve the last three equations (we define $\Delta\omega = \omega_e - \omega_{\text{MW}}$ for compactness):

$$\begin{aligned} \rho_{01}D &= -J^2V(\rho_{11} - \rho_{22}) + [V^3 + 2V(\Delta + i\gamma)(\Delta\omega + \Delta + i\gamma)](1 - 2\rho_{11} - \rho_{22}), \\ \rho_{02}D &= -JV(\Delta - \Delta\omega - i\gamma)(\rho_{11} - \rho_{22}) - 2JV(\Delta + i\gamma)(1 - 2\rho_{11} - \rho_{22}), \\ \rho_{12}D &= [J(\Delta\omega + \Delta + i\gamma)(\Delta\omega - \Delta + i\gamma) - J^3](\rho_{11} - \rho_{22}) - JV^2(1 - 2\rho_{11} - \rho_{22}), \\ D &= 2J^2(\Delta + i\gamma) + V^2(\Delta\omega - \Delta + i\gamma) - 2(\Delta + i\gamma)(\Delta\omega + \Delta + i\gamma)(\Delta\omega - \Delta + i\gamma). \end{aligned} \quad (\text{S100})$$

In the linear response regime, we seek $\rho_{01}, \rho_{02} = O(V)$, $\rho_{12}, \rho_{11}, \rho_{22} = O(V^2)$ and neglect V^2 in the denominator, which gives

$$\rho_{11} = \frac{V^2[(\Delta\omega + \Delta)^2 + \gamma^2]}{(\Delta\omega^2 - \Delta^2 - J^2 - \gamma^2)^2 + 4\gamma^2\Delta\omega^2}, \quad \rho_{22} = \frac{V^2J^2}{(\Delta\omega^2 - \Delta^2 - J^2 - \gamma^2)^2 + 4\gamma^2\Delta\omega^2}. \quad (\text{S101})$$

This is the expression plotted in the Fig. 2 in the main text. We have good mixing at $\gamma, \Delta \ll J$, Anderson localisation for $\gamma \ll J \ll \Delta$, Zeno localisation at $\Delta < J \ll \gamma$, and weak incoherent coupling for $J \ll \gamma, \Delta$.

V. MICROSCOPIC MODEL OF THE ELECTRONIC SPINS AND BATH

In this section we comment on the choice of the microscopic Hamiltonian of the whole system. However the present treatment of the dissipation modes is crude and does not allow to recover realistic orders of magnitudes for relaxation timescales ; nevertheless it shows a simple microscopic example with bath rates that are power-law increasing with temperature, as expected from NMR experiments.

A. Coupling between spins and the magnetic field

In absence of lattice vibrations, the electron spins are frozen in an amorphous matrix. We denote the position of a given spin by \mathbf{R} . The spin-orbit interaction between this spin and the external magnetic field depends on the orientation of the radical with respect to the field, and in general is thus written as a tensorial¹⁰ coupling $-g_{z\mu}\mu_B B S_i^\mu$ [49, Chap. VI]-[70] where

$$g_{z\mu} = g_e\delta_{z\mu} + g_{z\mu}^{(0)} \quad (\text{S102})$$

The first term in Eq. (S102) is the dominant isotropic contribution, resulting in the Zeeman part of the spin Hamiltonian H_S , *i.e.* $\sum_i \omega_e S_i^z = \omega_e S^z$ with $\omega_e = -g_e\mu_B B$ the Zeeman frequency, related to the electron Landé g -factor g_e ($\simeq -2$) through $\mu_B = \frac{e}{2m_e}$. e is the unit charge, m_e the electron mass and μ_B the Bohr magneton. In practice we take $\omega_e = 93.9 \cdot 2\pi\text{GHz}$, meaning $B \simeq 3.35$ Tesla, a standard value for DNP. The second term in Eq. (S102) is the so-called g -factor anisotropy of the disordered sample, which depends on the radical orientation and therefore appears as a random quantity. This term contributes to H_S as $\sum_i \Delta_i S_i^z$ with¹¹ $\Delta = -g_{zz}^{(0)}\mu_B B$. Note that we discarded directions $\mu \neq z$: when the magnetic field is large one can resort to the *secular* approximation of the Hamiltonian, which consists in keeping only the terms conserving the total polarization along z . The reason in that hybridization between different polarization sectors is very weak in perturbation theory [49, Chap. IV.II.A]-[42, 51].

¹⁰ Repeated Greek indices are summed over in the whole section.
Note that the magnetic field is along z , hence the z index.

¹¹ For notational simplicity we omit explicit reference to the spin i , implicitly born by $g_{zz}^{(0)}$.

B. Vibrational modes of the embedding material

The position of an electron spin in the amorphous matrix is $\mathbf{r} = \mathbf{R} + \mathbf{u}(\mathbf{R})$ with \mathbf{R} an equilibrium position, and $\mathbf{u}(\mathbf{R})$ describes a small vibrational motion around it. The latter motion affects all space-dependent quantities, such as the Zeeman interaction which is the strongest term in the Hamiltonian. The field \mathbf{u} is expected to vary slowly on the scale of the electron distances for extended vibrational modes. The distance between two particles 1 and 2 in the matrix is indeed $\mathbf{r} = \mathbf{r}_1 - \mathbf{r}_2 = \mathbf{R}_1 - \mathbf{R}_2 + (\partial_\mu \mathbf{u})(\mathbf{R}_1 - \mathbf{R}_2)_\mu$ at first order in the \mathbf{u} derivatives. The tensorial coupling in Eq. (S102) is now modified by the vibrations as [71, Chap. 22]-[72].

$$g_{z\mu} = g_e \delta_{z\mu} + g_{z\mu}^{(0)} + g_{z\mu\gamma\delta}^{(1)} \partial_\gamma u^\delta + g_{z\mu\gamma\delta\gamma'\delta'}^{(2)} \partial_\gamma u^\delta \partial_{\gamma'} u^{\delta'} + \dots \quad (\text{S103})$$

Vibrational modes in the glass originate from several processes [73, 74], but in the following we shall restrict ourselves for simplicity to model them as low-energy excitations arising from acoustic phonon modes¹². In the glassy sample, the arrangement of the different atoms is not periodic. This implies a continuous set of wavevectors; we nevertheless use the standard theory of phonons of a periodic lattice for convenience, as it should not affect much the results. One can write the quantized displacement field [71]

$$\mathbf{u}(\mathbf{R}) = \frac{1}{\sqrt{N}} \sum_{\mathbf{k}, s} \frac{\mathbf{e}_{\mathbf{k}/k, s}}{\sqrt{2m\Omega_{\mathbf{k}, s}}} a_{\mathbf{k}, s} e^{i\mathbf{k}\cdot\mathbf{R}} + \text{H.c.} \quad (\text{S104})$$

$s = 1, 2, 3$ is the polarization index, \mathbf{k} are the wavevector (quantized in the first Brillouin zone due to the assumed periodicity of the lattice), m is the mass of the glassy molecule¹³ $\Omega_{\mathbf{k}, s}$ are the phonon frequencies, $\mathbf{e}_{\mathbf{k}/k, s}$ are polarization unit eigenvectors, and $a_{\mathbf{k}, s}$, $a_{\mathbf{k}, s}^\dagger$ are phonon annihilation and creation operators. The bath Hamiltonian is thus a collection of harmonic oscillators $H_B = \sum_{\mathbf{k}, s} \Omega_{\mathbf{k}, s} a_{\mathbf{k}, s}^\dagger a_{\mathbf{k}, s}$.

In the following we consider separately the one- and two-phonon processes as they are incoherent owing to Wick's theorem [67], *i.e.* their contribution to the correlation function $\langle B_i^\mu(t) B_i^\mu \rangle_B$ is additive.

1. Direct process

The direct process concerns the exchange of a single phonon between the bath and the system. It is due to the first-order interaction between the spin and the bath modes in Eq. (S103) involving the tensor $g^{(1)}$, substituting $\partial_\gamma u^\delta$ via Eq. (S104). The interaction Hamiltonian is thus of the form (S2) where B_i^μ a linear combination of annihilation and creation operators. The equilibrium bath correlation function (S15) then involves only quadratic correlators in the $a_{\mathbf{k}, s}$. For simplicity we drop tensor indices and the polarization vectors, as these factors only contribute $O(1)$ proportionality constants. The calculation is standard (see (S87)-(S88)) using the dispersion relation $\Omega_k = kv$ with v the sound velocity. We get in the continuous limit $N \rightarrow \infty$

$$\frac{1}{T(|\omega|)} = \frac{1}{2\pi} \left(\frac{g^{(1)}}{g_e} \right)^2 \frac{\omega_e^2}{\rho_0 v^5} \omega^3 \coth \left(\frac{\beta\omega}{2} \right) \quad (\text{S105})$$

where $\rho_0 = Nm/L^3$ is the mass density.

2. Two-phonon processes

The next term in the system-bath interaction is a two-phonon process caused by the second-order interaction between the spin and the bath modes in Eq. (S103) involving the tensor $g^{(2)}$. It takes the form (S2) where B_i^μ is quadratic in the annihilation and creation operators. We thus have to deal with 4-point canonical averages applying Wick's theorem [67]. In the continuous limit for wavevectors and at low temperature¹⁴, dropping again indices and polarization vectors, we obtain

$$\frac{1}{T(|\omega|)} = \frac{16}{\pi^3} \left(\frac{g^{(2)}}{g_e} \right)^2 \frac{\omega_e^2}{(\rho_0 v^5)^2} T^7 \cosh \left(\frac{\beta\omega}{2} \right) \left[\underbrace{\int_0^{\beta|\omega|/2} dy \frac{y^3 \left(\frac{\beta|\omega|}{2} - y \right)^3}{\sinh y \sinh \left(\frac{\beta|\omega|}{2} - y \right)}}_{\text{absorption of two phonons}} + \underbrace{2 \int_0^\infty dy \frac{y^3 \left(\frac{\beta|\omega|}{2} + y \right)^3}{\sinh y \sinh \left(\frac{\beta|\omega|}{2} + y \right)}}_{\text{Raman process: absorption and emission}} \right] \quad (\text{S106})$$

¹² One may expect this physical picture to dominate the system-bath interaction at low temperature for energies below 100 GHz, based on Fermi's golden rule which involves vibrational

density of states estimates from Refs. [73, 74].

¹³ *i.e.* approximating pyruvic acid as a monoatomic substance.

¹⁴ The Debye frequency Ω_D must be large, *i.e.* $\beta\Omega_D \gg 1$.

3. Discussion of the one- and two-phonon bath timescales

For our range of frequencies and temperature, the direct rate (S105) is $\propto \omega^2 T$. The two-phonon contribution (S106) is dominated by the Raman contribution roughly independent of the frequency and $\propto T^7$. In experiments the dependence in frequency is not known while the dependence in temperature of $T_1 = 2T(\omega_e)$ is roughly T^2 [75, 76]. As we do not know realistic values of the ratios $g^{(i)}/g_e$, we cannot assess the order of magnitude of the predicted timescales, as well as the relative weight of the Raman rate with respect to the direct rate which determines the temperature dependence of the bath correlation function $\gamma(\omega)$. Yet it is known experimentally that the relaxation time T_1 of the system is ~ 1 s at $\beta^{-1} \sim 1$ K, which implies gigantic orders of magnitude for the unknown quantities $g^{(i)}/g_e$. Finally let us look at the decorrelation assumption of the bath degrees of freedom. The fact that $\langle B_i^\mu(t) B_j^\nu \rangle_B \propto \delta_{\mu\nu}$ owes to the isotropy of the material. If $i \neq j$ the only difference is that all integrals over wavevectors (say \mathbf{k}) get an additional phase factor $e^{i\mathbf{k}\cdot(\mathbf{R}_i - \mathbf{R}_j)}$. Therefore decorrelation happens if the wavelength of the phonon is much smaller than the inter-electron distance $|\mathbf{R}_i - \mathbf{R}_j|$. In other words, the criterion for decorrelation is that the phonon frequencies ω involved are such that $\omega \gg v/|\mathbf{R}_i - \mathbf{R}_j|$ i.e. $\omega \gg v\rho_e^{1/3}$ where ρ_e is the electron density in the material. In practice ($\rho_e \sim 10$ mmol/L, $v \sim 10^3$ m/s) this threshold is of the same order of magnitude as ω_e . We conclude that this model of ballistic phonons does not give a realistic description but represents a simple example with a power-law decrease of the bath relaxation timescales needed for Zeno localization.

[1] L. D'Alessio, Y. Kafri, A. Polkovnikov, and M. Rigol, *Advances in Physics* **65**, 239 (2016).

[2] E. M. Lifshitz and L. P. Pitaevskii, *Statistical Physics, Part 2*, vol. 9 of *L. D. Landau and E. M. Lifshitz Course of Theoretical Physics* (Pergamon Press, 1980), sec. 41.

[3] J. M. Deutsch, *Physical Review A* **43**, 2046 (1991).

[4] M. Srednicki, *Physical Review E* **50**, 888 (1994).

[5] R. Nandkishore and D. A. Huse, *Annual Review of Condensed Matter Physics* **6**, 15 (2015).

[6] F. Alet and N. Laflorencie, *Comptes Rendus Physique* **19**, 498 (2018), ISSN 1631-0705, quantum simulation / Simulation quantique.

[7] D. A. Abanin, E. Altman, I. Bloch, and M. Serbyn, *Reviews of Modern Physics* **91** (2019).

[8] B. L. Altshuler, Y. Gefen, A. Kamenev, and L. S. Levitov, *Phys. Rev. Lett.* **78**, 2803 (1997).

[9] D. M. Basko, I. L. Aleiner, and B. L. Altshuler, *Annals of Physics* **321**, 1126 (2006), ISSN 0003-4916.

[10] M. Pollak and B. Shklovskii, eds., *Hopping Transport in Solids*, vol. 28 of *Modern Problems in Condensed Matter Sciences* (Elsevier, 1991).

[11] A. Beskow and J. Nilsson, *Arkiv für Fysik* **34**, 561 (1967).

[12] L. Khalfin, *Jetp Lett.* **8**, 65 (1968).

[13] B. Misra and E. C. G. Sudarshan, *Journal of Mathematical Physics* **18**, 756 (1977).

[14] W. M. Itano, D. J. Heinzen, J. J. Bollinger, and D. J. Wineland, *Phys. Rev. A* **41**, 2295 (1990).

[15] P. Facchi and S. Pascazio, in *Progress in Optics* (Elsevier, 2001), pp. 147–217.

[16] H.-P. Breuer and F. Petruccione, *The theory of open quantum systems* (Oxford University Press, 2002).

[17] D. A. Huse, R. Nandkishore, F. Pietracaprina, V. Ros, and A. Scardicchio, *Physical Review B* **92**, 014203 (2015).

[18] V. S. Shchesnovich and V. V. Konotop, *Phys. Rev. A* **81**, 053611 (2010).

[19] P. Barmettler and C. Kollath, *Phys. Rev. A* **84**, 041606 (2011).

[20] D. A. Zezyulin, V. V. Konotop, G. Barontini, and H. Ott, *Phys. Rev. Lett.* **109**, 020405 (2012).

[21] H. Fröml, A. Chiocchetta, C. Kollath, and S. Diehl, *Phys. Rev. Lett.* **122**, 040402 (2019).

[22] P. E. Dolgirev, J. Marino, D. Sels, and E. Demler, *Phys. Rev. B* **102**, 100301 (2020).

[23] A. J. Bray and M. A. Moore, *Phys. Rev. Lett.* **49**, 1545 (1982).

[24] S. Chakravarty, *Phys. Rev. Lett.* **49**, 681 (1982).

[25] A. Schmid, *Physical Review Letters* **51**, 1506 (1983).

[26] A. J. Leggett, S. Chakravarty, A. T. Dorsey, M. P. A. Fisher, A. Garg, and W. Zwerger, *Reviews of Modern Physics* **59**, 1 (1987).

[27] L. F. Cugliandolo, D. R. Grempel, G. Lozano, H. Lozada, and C. A. da Silva Santos, *Physical Review B* **66**, 014444 (2002).

[28] Y. Li, X. Chen, and M. P. A. Fisher, *Phys. Rev. B* **98**, 205136 (2018).

[29] A. Chan, R. M. Nandkishore, M. Pretko, and G. Smith, *Phys. Rev. B* **99**, 224307 (2019).

[30] B. Skinner, J. Ruhman, and A. Nahum, *Phys. Rev. X* **9**, 031009 (2019).

[31] M. Szyniszewski, A. Romito, and H. Schomerus, *Phys. Rev. B* **100**, 064204 (2019).

[32] X. Turkeshi, R. Fazio, and M. Dalmonte, *Phys. Rev. B* **102**, 014315 (2020).

[33] C.-M. Jian, Y.-Z. You, R. Vasseur, and A. W. W. Ludwig, *Phys. Rev. B* **101**, 104302 (2020).

[34] A. Zabalo, M. J. Gullans, J. H. Wilson, S. Gopalakrishnan, D. A. Huse, and J. H. Pixley, *Phys. Rev. B* **101**, 060301 (2020).

[35] Y. Bao, S. Choi, and E. Altman, *Phys. Rev. B* **101**, 104301 (2020).

[36] L. Zhang, J. A. Reyes, S. Kourtis, C. Chamon, E. R. Mucciolo, and A. E. Ruckenstein, *Phys. Rev. B* **101**, 235104 (2020).

[37] X. Cao, A. Tilloy, and A. D. Luca, *SciPost Phys.* **7**, 24 (2019).

[38] Q. Tang and W. Zhu, *Phys. Rev. Research* **2**, 013022 (2020).

[39] S. Goto and I. Danshita, *Phys. Rev. A* **102**, 033316 (2020).

[40] Y. Fuji and Y. Ashida, *Phys. Rev. B* **102**, 054302 (2020).

[41] A. De Luca and A. Rosso, *Physical review letters* **115**, 080401 (2015).

[42] A. D. Luca, I. Rodríguez-Arias, M. Müller, and A. Rosso, *Physical Review B* **94**, 014203 (2016).

[43] I. Rodríguez-Arias, M. Müller, A. Rosso, and A. De Luca, *Phys. Rev. B* **98**, 224202 (2018).

[44] Z. Lenarčič, E. Altman, and A. Rosch, *Physical Review Letters* **121** (2018).

[45] Z. Lenarčič, O. Alberton, A. Rosch, and E. Altman, *Phys. Rev. Lett.* **125**, 116601 (2020).

[46] F. Lange, Z. Lenarčič, and A. Rosch, *Nature Communications* **8** (2017).

[47] D. Guarin, S. Marhabaie, A. Rosso, D. Abergel, G. Bodenhausen, K. L. Ivanov, and D. Kurzbach, *The Journal of Physical Chemistry Letters* **8**, 5531 (2017).

[48] V. Atsarkin, *Soviet Phys.-JETP* **31**, 1012 (1970).

[49] A. Abragam, *The principles of nuclear magnetism*, 32 (Oxford university press, 1961).

[50] A. Abragam and M. Goldman, *Reports on Progress in Physics* **41**, 395 (1978).

[51] S. A. Smith, W. E. Palke, and J. T. Gerig, *Concepts in Magnetic Resonance* **4**, 107 (1992).

[52] F. Bloch, *Physical Review* **70**, 460 (1946).

[53] P. Schosseler, T. Wacker, and A. Schweiger, *Chemical Physics Letters* **224**, 319 (1994).

[54] J. Granwehr and W. Köckenberger, *Applied Magnetic Resonance* **34**, 355 (2008).

[55] Y. Hovav, I. Kaminker, D. Shimon, A. Feintuch, D. Goldfarb, and S. Vega, *Physical Chemistry Chemical Physics* **17**, 226 (2015).

[56] R. Alicki, *Physical Review A* **40**, 4077 (1989).

[57] R. Alicki, D. Gelbwaser-Klimovsky, and G. Kurizki, *arXiv:1205.4552* (2012).

[58] F. Nathan and M. S. Rudner, *Phys. Rev. B* **102**, 115109 (2020).

[59] G. Kiršanskas, M. Franckié, and A. Wacker, *Physical Review B* **97** (2018).

[60] E. Kleinherbers, N. Szpak, J. König, and R. Schützhold, *Phys. Rev. B* **101**, 125131 (2020).

[61] Y. Hovav, A. Feintuch, and S. Vega, *Phys. Chem. Chem. Phys.* **15**, 188 (2013).

[62] J. Bezanson, A. Edelman, S. Karpinski, and V. B. Shah, *SIAM Review* **59**, 65 (2017), <https://doi.org/10.1137/141000671>.

[63] Y. Saad, *Iterative Methods for Sparse Linear Systems* (Society for Industrial and Applied Mathematics, 2003).

[64] N. Pottier, *Nonequilibrium statistical physics: linear irreversible processes* (Oxford University Press, 2010).

[65] M. Le Bellac, *Physique quantique* (EDP sciences, 2012).

[66] I. Rodríguez-Arias, A. Rosso, and A. D. Luca, *Magnetic Resonance in Chemistry* **56**, 689 (2018).

[67] P. Coleman, *Introduction to Many-Body Physics* (Cambridge University Press, 2015).

[68] F. Caracciolo, M. Filibian, P. Carretta, A. Rosso, and A. D. Luca, *Physical Chemistry Chemical Physics* **18**, 25655 (2016).

- [69] S. C. Serra, M. Filibian, P. Carretta, A. Rosso, and F. Tedoldi, *Phys. Chem. Chem. Phys.* **16**, 753 (2014).
- [70] L. F. Chibotaru, A. Ceulemans, and H. Bolvin, *Phys. Rev. Lett.* **101**, 033003 (2008).
- [71] N. W. Ashcroft and N. D. Mermin, *Solid state physics* (Holt, Rinehart and Winston, 1976).
- [72] L. D. Landau and E. M. Lifshitz, *Theory of Elasticity* (Elsevier, 1986).
- [73] H. Mizuno, H. Shiba, and A. Ikeda, *Proceedings of the National Academy of Sciences* **114**, E9767 (2017).
- [74] L. Wang, A. Ninarello, P. Guan, L. Berthier, G. Szamel, and E. Flenner, *Nature Communications* **10** (2019).
- [75] M. Filibian, S. C. Serra, M. Moscardini, A. Rosso, F. Tedoldi, and P. Carretta, *Phys. Chem. Chem. Phys.* **16**, 27025 (2014).
- [76] M. Filibian, E. Elisei, S. C. Serra, A. Rosso, F. Tedoldi, A. Cesàro, and P. Carretta, *Physical Chemistry Chemical Physics* **18**, 16912 (2016).